Mirror Symmetry Breaking and Chiral Amplification of Ethylenediammonium Sulfate Crystals

Pui Shan Monica Cheung

A Thesis

in

The Department

of

Chemistry and Biochemistry

Presented in Partial Fulfillment of the Requirements
for the Degree of Master Science (Chemistry) at
Concordia University
Montréal, Québec, Canada

August 2008

Your file Votre référence
ISBN: 978-0-494-45334-6
Our file Notre référence
ISBN: 978-0-494-45334-6

ABSTRACT

Mirror Symmetry Breaking and Chiral Amplification of Ethylenediammonium Sulfate Crystals

Pui Shan Monica Cheung

Chiral symmetry breaking is a process that generates one enantiomer largely over the other when a racemic mixture is expected. In nature, one handedness is preferred over the other and it has been shown that chiral molecules, including amino acids, can preferentially adsorb on chiral mineral surfaces such as quartz and calcite. This project investigates the mirror symmetry breaking process of ethylenediammonium sulfate (EDS), an achiral salt that crystallizes into chiral crystals. Here, we investigate the directed mirror symmetry breaking and chiral amplification of EDS in the presence of chiral amino acids using an abrasion/grinding process. The direction of chiral symmetry breaking is strongly dependent on the amino acid and its chirality: (*i*) for thirteen chiral amino acids, the addition of the D-isomer directed the chiral symmetry breaking process towards homochiral *dextrorotatory* EDS crystals; whereas the addition of the L-isomer directed the chiral symmetry breaking process towards homochiral *levorotatory* EDS crystals, (*ii*) asparagine, tryptophan and tyrosine showed the reverse trend, and (*iii*) no effect was observed when adding arginine, lysine or methionine to the EDS mixture. In the future, the effect of chiral additives on the surface microtopography of EDS crystals will be investigated using atomic force microscopy and surface etching. The selective adsorption of chiral additives on EDS crystals will also be studied using molecular modeling and isothermal titration calorimetry.

Acknowledgement

I would like to express my deepest gratitude to my supervisor, Dr. Louis Cuccia, for his guidance, patience and encouragement throughout my graduate study. For the past few years, Louis has been a dear friend and I would have not been able to accomplish as much in my academic career without his help. I would like to thank my parents and my sister for their endless love and support. I would like to thank Dr. Christine DeWolf, Dr. Yves Gélinas and Dr. Chris Wilds for serving on my research committee. I especially would like to thank my dear friends, Marta and Carolin, for sharing many wonderful times together. Also, I would like to give a million thanks to Dr. Rolf Schmidt for his time proofreading my thesis, sharing his expertise and giving valuable comments during exceptionally early group meetings. I thank all other colleagues who have helped me during my stay at Concordia; especially Jacinthe, Jamie, Ye, and Wendy for their contribution to this research project. I thank Dr. Jean-Marie Lehn for the inspiration leading to this project. I thank Dr. Joanne Turnbull and Dr. Paul Joyce for providing material needed for this study, Dr. Bruce Lennox and Dr. Peter Pawelek for useful advice and access to instrumentation, Dr. Cameron Skinner and Dr. Christopher Barrett for useful discussions, Dr. Guillaume Lamoureux for his assistance in molecular modeling and for writing the corresponding experimental section, Dr. Jeanne Paquette and Dr. Scott Bohle for helpful discussions on crystallography, Dr. Cristobal Viedma, Dr. Pedro Cintas and Dr. Donna Blackmond for valuable discussions and comments on chiral symmetry breaking, Dr. Yitzhak Mastai for his help with isothermal titration calorimetry experiments, Dr. Venkataramanan Mahalingam and Rafik Naccache for their help with x-ray powder diffraction experiments and Richard Allix for technical expertise. I am very

lucky to have had the opportunity to thank so many people for helping me throughout my study at Concordia. Thank you ☺

My lovely family at home

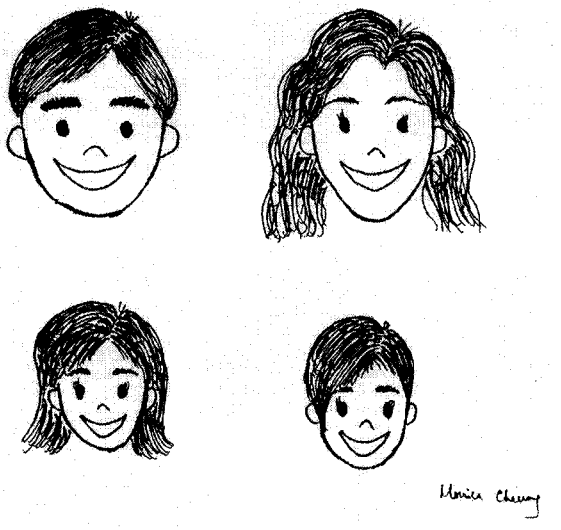

My lovely family at school

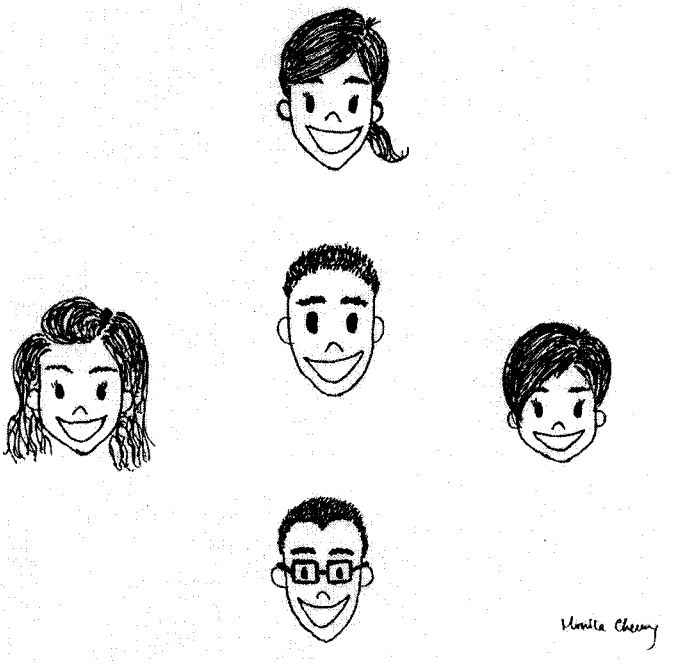

Charlie's Angels

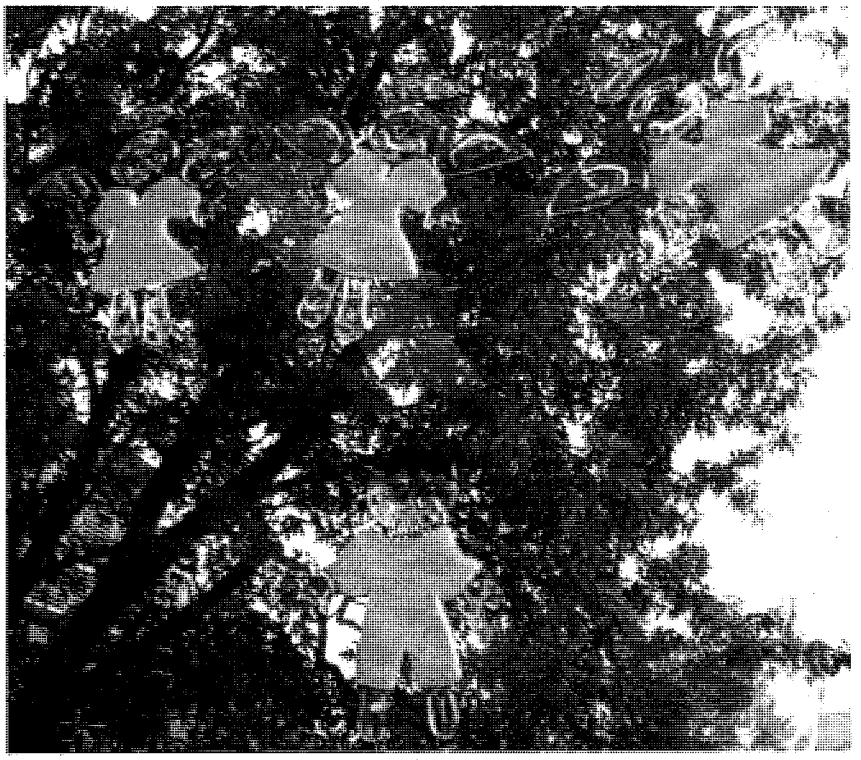

Table of Contents

List of Figures

List of Tables

List of abbreviations

Abbreviation	Description
aa	Amino acid
AFM	Atomic force microscopy
CEE	Crystal enantiomeric excess
CHARMM	Chemistry at HARvard Macromolecular Mechanics
CPL	Circularly polarized light
DIC	Dye inclusion crystal
E_{bind}	Binding energy
EDS	Ethylenediammonium sulfate
EE	Enantiomeric excess
ITC	Isothermal titration calorimetry
ORD	Optical rotatory dispersion
PVED	Parity violation energy difference
rpm	Revolution per minute
xtl	Crystal

List of special symbols

Special symbol	Description
( )	Miller index notation for one face
{ }	Miller index notation for a set of symmetry equivalent faces. *e.g.* $\{100\}$ faces for a tetragonal prism indicates the (100), (010), $(\bar{1}00)$, and $(0\bar{1}0)$ faces
[ ]	Vector direction or edge

Chapter 1. Introduction

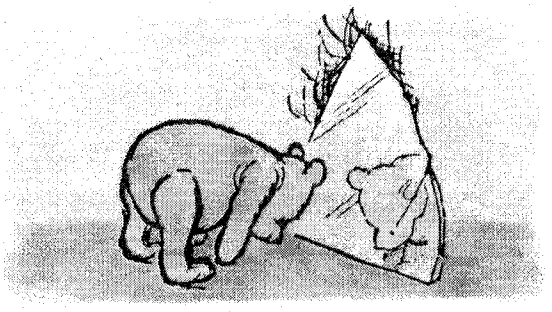

Pooh looked at his two paws. He knew that one of them was the right, and he knew that when you had decided which one of them was the right, then the other one was the left, but he never could remember how to begin.

The House at Pooh Corner

A.A. Milne

1.1. Origin of homochirality

How, when and where did life first appear on earth? Life is believed to have originated around 3.5 billion years ago.[1] Several hypotheses on the emergence of life have been proposed; for example, (*i*) the classical 'prebiotic soup' containing simple abiotic building blocks that evolve towards complexity – Darwin's model[2], (*ii*) the metabolic reaction cycles that occur on mineral surfaces under an iron-sulfur rich environment allow for the formation of peptides – the 'iron-sulfur world' theory[3], and (*iii*) an evolution of RNA molecules, responsible for genetic information storage and reaction catalysis, which further developed into DNA molecules and proteins – the 'RNA world' model[4]. The chemical basis of these theories has evolved in a similar fashion; it begins with simple building blocks which self-organize spontaneously into more complex forms. Unfortunately, none of the proposed hypotheses are conclusive. Furthermore, the mystery behind the origin of life can not be untangled without addressing the possible origins of homochirality (*i.e.* homochirogenesis), where nature has chosen to thrive in a chiral rather than a racemic environment.[5]

In nature, one handedness is preferred over the other; the key examples are D-sugars and L-amino acids. More importantly, the genetic information of living organisms is stored in right-handed β-DNA. Clearly, chirality preference plays an essential role in living systems. Different theories have been suggested to explain the appearance of chiral preference in nature. One of the hypotheses is parity violation in weak interactions proposed by Lee and Yang in 1956,[6] and later confirmed experimentally by Wu *et al.* in 1957.[7] The experiment consisted of measuring the emission of β-particles (electrons) from a radioactive ^{60}Co sample under a magnetic field at low temperature. Due to the parity violation energy difference (PVED) during β-decay, an excess of electron spins antiparallel to the direction of propagation (left-handed spins) was observed as opposed to mirror symmetry of electron emission. Circularly polarized light (CPL) is also believed to be a potential cause of the chirality imbalance in nature.[5] Within a narrow wavelength range, a slight excess of left-CPL is produced before sunrise and a slight excess of right-CPL is produced after sunset.[8] Although these two excesses of CPL are expected to cancel each other out, irregular landscapes may cause uneven exposure of CPL in localized areas.[9] Cosmic meteorites are also proposed as a possible source of introducing chiral impurities on earth and evidence has shown that some carbonaceous chondrites contain the essential building blocks of life such as organic carbon, amino acids and nucleic acid bases.[10, 11] However, this only expands the mystery behind the origin of homochirality from earth to the universe. Several studies have reported enantioselective adsorption of chiral molecules on chiral mineral surfaces such as quartz[12], calcite[13] and gypsum.[14] The preferential adsorption of one enantiomorphous

form of a molecule over the other on chiral mineral surfaces might have played an important role in chiral selection in the prebiotic environment.[15]

1.2. Stereochemistry

Molecular handedness is the center of attention in chemistry for seeking an answer to the origin of homochirality. Any object or molecule lacking an improper rotation axis (*i.e.* mirror plane and inversion center) is considered to be chiral.[16] Chiral objects or molecules are non-superposable on their mirror images, and molecules that are non-superposable mirror images of each other are called enantiomers. In stereochemistry, specific notations are assigned to describe the three-dimensional arrangement of atoms in a chiral molecule. A summary of symmetry elements, including improper rotation axes, is provided in Table 1.[16]

Table 1. Summary of symmetry elements.[16]

Symmetry operation	Notation	Description
Rotation axis	C_n	An axis about which a molecule rotates; n = number of identical positions around the axis
Mirror plane	σ	A plane that divides a molecules into two halves that are mirror images
Inversion center	i	A point through which the molecule is inverted
Improper rotation axis	S_n	Rotate by 360°/n along the axis followed by a reflection in a plane perpendicular to the axis

1.2.1. Handedness and chirality

In the macroscopic world, chiral objects are abundant in our surroundings *e.g.* our hands, screws, and spiral sea shells.[5] At the molecular level, the simplest chiral molecule is a tetrahedral carbon atom with four different substituents. The handedness of this

stereogenic center is assigned depending on the three-dimensional arrangement of the substituents and the priority assigned to these substituents. Different terminologies have been established to classify the configuration of chiral molecules.

In the Cahn-Ingold-Prelog (CIP) convention, *R* (Latin *'rectus'*) and *S* (Latin *'sinister'*) are assigned to chiral molecules with a stereogenic center according to the atomic number of the attached substituents. The CIP rule is executed by positioning the lowest priority group away from the observer and tracing the priorities of the remaining substituents in descending order either clockwise or counterclockwise. The clockwise direction is assigned to have the *R* configuration and the counterclockwise direction is assigned to have the *S* configuration.[17]

In 1891, Emil Fischer developed a stereochemical nomenclature especially for sugars and amino acids that is still used today.[18] This nomenclature uses the prefixes D and L and is based on the stereochemistry of glyceraldehyde as a reference compound (Figure 1). To use this nomenclature, the molecular structure of the sugar or amino acid has to be positioned in a Fischer projection with the most highly oxidized carbon atom placed on the top of the vertically aligned carbon backbone. For sugars, the designator D is assigned when the hydroxy group on the lowest stereogenic center is located on the right side of the carbon backbone; whereas L is assigned when this hydroxy group is located on the left side (Figure 1). A similar system is used for assigning the chirality of amino acids, except that the left or right orientation of the amino group is considered instead of a hydroxy group (Figure 1).[16]

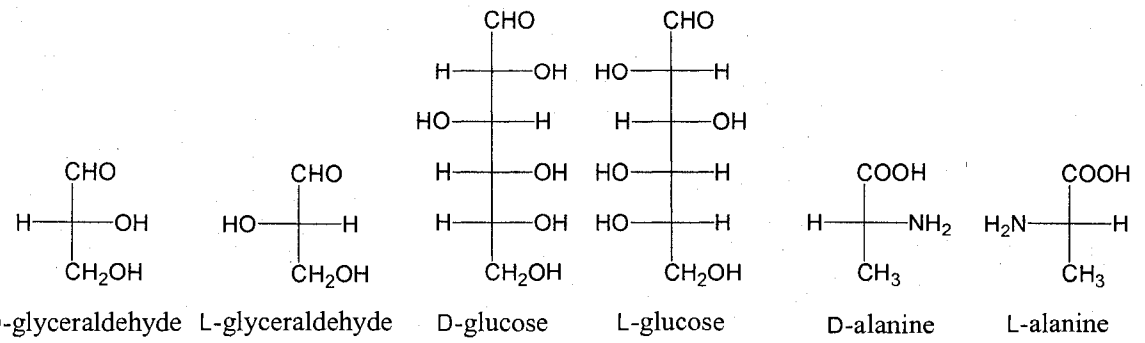

Figure 1. Fischer projections of the enantiomeric pairs of glyceraldehyde, glucose and alanine.

The prefixes *d* (*dextrorotatory* or +) and *l* (*levorotatory* or –) are absolute descriptors used for chiral molecules based on the direction in which they rotate plane polarized light.[19] To determine the rotation direction of plane polarized light through a chiral medium, a pair of polarizing filters can be used. When white light passes through the first polarizing filter (the polarizer), the light waves are aligned parallel to the orientation of the polarizing filter. When passing through a chiral medium, this plane of polarization is rotated. Since the light waves are oriented at a different angle, the second polarizing filter (the analyzer) can be used to reorient the light in a parallel direction to obtain a maximum intensity of light transmission. A chiral sample is *d* if the plane polarized light is rotated in a clockwise (right-handed) direction and a chiral sample is *l* if the plane polarized light is rotated in a counterclockwise (left-handed) direction. Any media (solid, liquid or gas) that is capable of rotating plane polarized light is optically active.[20] The degree of rotation of plane polarized light depends on several factors including the wavelength of the light, the temperature, the concentration of the sample and the path length of the polarimeter cell. The specific rotation, $[\alpha]_D^t$, can be determined using a polarimeter and has units of deg cm^2 g^{-1} according to equation 1:

$$[\alpha]_D^t = \frac{\alpha}{l \times c} \quad (1)$$

where α is the observed rotation (°), l is the length of the polarimeter cell (dm); c is the concentration (g cm^{-3}), t is the temperature (°C) and D corresponds to the sodium D line at 589.6 nm.[21] Figure 2 shows a vintage Goerz polarimeter with a 1 dm polarimeter cell.

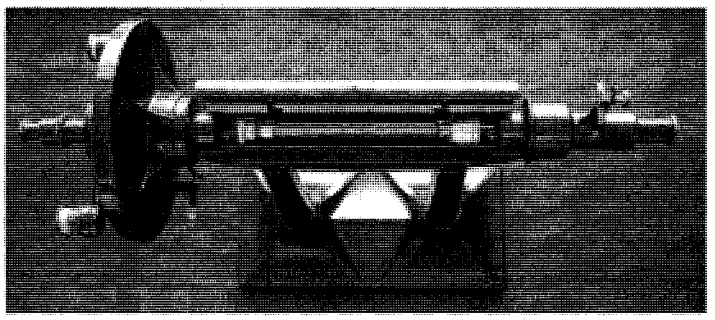

Figure 2. A vintage Goerz polarimeter.

1.2.2. Optical rotatory dispersion (ORD)

Another manifestation of the rotation of plane polarized light is the color change of chiral samples under a polarizing microscope. In 1812, Biot reported an increase in the angle of rotation of plane polarized light by quartz as the color of the light changed from red (long wavelength) to violet (short wavelength).[19] Therefore, when plane polarized light passes through a chiral sample, changes in color of the transmitted light are observed as the analyzer is rotated. This dependence of specific rotation on wavelength is called optical rotatory dispersion (ORD).[22]

1.3. Crystallography

ORD is an important feature of chiral samples that are in the crystalline state because the velocity of the light transmission through a crystal depends on its crystallographic symmetry.[23] In brief, there are three basic elements of symmetry in crystallography: (*i*) a center of inversion is the meeting point where all crystal faces on one side are identical to the parallel crystal faces at the opposite side, (*ii*) a plane of symmetry (parallel to a crystal face or diagonally through a crystal) that divides a crystal into two identical portions which are mirror images of each other with respect to the plane and (*iii*) an axis of symmetry is an imaginary line where a rotation is executed along the axis until the identical position is met.

1.3.1. Unit cell

The smallest volume element that is repeated in three dimensions to give a crystal is known as the unit cell.[24] Each unit cell is composed of molecules that are arranged in three-dimensional space. The dimensions of a unit cell are indicated by the translation axes (a, b, and c) as shown in Figure 3. The number Z indicates the number of molecules contained in a unit cell.

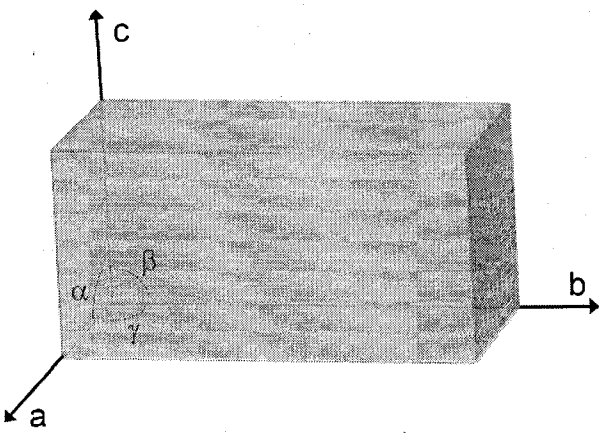

Figure 3. Schematic representation of a unit cell. Arrows represent translational axes and arcs represent angles between the axes.

1.3.2. Miller indices

Miller indices are the notation used to identify the crystal faces through the translational vector in three-dimensional space.[24] The unit length assigned to each axis represents the unit length in angstroms (Å) from the origin and the positive or negative sign represents the direction of the axis. A crystal face is indexed when a plane is drawn across the three Cartesian coordinates. The spacing in crystals is defined by the crystallographic planes characteristic for a particular crystal (*i.e.* the *h*, *k*, *l* Miller indices which are the reciprocal of the relative intercepts on the three crystallographic axes). If a zero results from the reciprocal of a relative intercept, it indicates that the plane will not intercept that particular axis. The atoms in a crystal are arranged in a regular pattern and can diffract an x-ray beam. In a crystalline powder there is a random distribution of all possible orientations and only crystallites having crystallographic planes (*h*, *k*, *l*) parallel to the specimen surface will contribute to the reflected intensities.[24]

Bragg's law (equation 2) can be used to determine interatomic spacings within a crystal:[24]

$$n\lambda = 2d \cdot \sin\theta \qquad (2)$$

where n is an integer, λ is the wavelength of the x-ray radiation (1.54 Å for a copper source), *d* is the interatomic spacing (Å) and θ is the diffraction angle (°). The possible θ values for reflections are determined by the unit cell dimensions and the intensities of the reflections are determined by the distribution of the electrons in the unit cell.

1.3.3. Crystal systems, Bravais lattices and crystallographic point groups

Crystals are grouped based on their symmetry into seven crystallographic systems: triclinic, monoclinic, orthorhombic, cubic, trigonal, tetragonal, and hexagonal. There are classes (*i.e.* point groups) within each of these crystallographic systems where symmetry allows for a crystalline structure to be chiral and optically active. Some crystals are isotropic (*e.g.* cubic crystals) because the arrangement of molecules is identical along the three axes within the crystal so that light is transmitted equally in all directions. On the other hand some crystals are anisotropic (*e.g.* tetragonal crystals) because the arrangement of molecules is different along the axes so that light is transmitted differently through the crystal. Based on the fundamental crystallographic systems, the unit cells are organized in a repetitive manner into fourteen geometric shapes in three-dimensional space. These crystal shapes are called Bravais lattices.[24] The imaginary points (nodes) in the Bravais lattices indicate the location of identical environments and coincide with positions of elements of symmetry. Each point experiences an identical environment as its neighbours. The lattice point arrangement becomes more complex as the combination of symmetry elements present increases. The location of the lattice points is described by the following notations: *P* (*primitive*) indicates that nodes are located at the corners, *I* (German: *Innenzentriert* or *body-*

centered) indicates an additional central point, *F* (*face-centered*) indicates an additional central point of all lattice faces, and *C* (*side-centered*) indicates an additional central point at only one pair of the unit cell faces. A crystallographic point group indicates the fix point (at least one) that is shared by the symmetry elements of a molecule.[24] The combination of the Bravais lattices and point groups describes the arrangements of atoms in three-dimensional space. These 230 space arrangements are called space groups and 65 of these space groups are chiral. An example of a chiral space group is $P4_1$. It is part of the tetragonal crystallographic system and is described in a *primitive* crystal lattice family. Any part of the atomic pattern is repeated in space by a 90° rotation and will meet its next identical unit if this rotation along the tetrad axis (parallel to the c-axis) is followed by a translation of ¼ of the unit length of the c-axis.[23]

1.3.4. Crystal growth and crystal habit

The crystallographic description of a structure provides details on the molecular arrangement in the crystalline state; however, it does not predict the macroscopic shape of the resulting crystal. The polyhedral forms of a crystal (*i.e.* crystal morphology) are influenced by other factors such as the crystal growth conditions and the crystal growth rate. 'Habit' is the term used to describe the overall growth form of individual crystals.[25]

Crystal growth is a thermodynamic process where molecules self-assemble into a regular pattern. However, crystal growth and dissolution requires a driving force and the Miers region is known to be the area where crystal growth and nucleation are unfavoured. The occurrence of growth and dissolution can be triggered by varying parameters such as concentration, temperature, and pressure.[25] The crystal surface is an important area of a crystal because it is the location where crystal growth and dissolution occur. Once the

energy barrier is surpassed, the crystal nucleus will form when a crystal cluster reaches a critical size (r_c) and the crystallizing particles will continue to associate at the crystal surface. This process of nucleation from solution is called primary nucleation. When a solvated solute binds to the crystal surface, desolvation occurs and the solute concentration at the solution-crystal interface decreases. The concentration gradient will lead to solution diffusion to maintain the bulk concentration at equilibrium (bulk diffusion). Conversely, the molecules or ions leave the crystal surface during dissolution and their concentration at the solution-crystal interface increases. In the case of an initial mother crystal broken into smaller crystallites, the resulting crystalline seeds serve as nucleation sites which grow into larger crystals of the same chirality as the mother crystal. This crystal growth process is called secondary nucleation.[25]

The crystal habit is related to the relative rate of crystal growth at different crystal faces. A crystal face with a slower normal growth rate (k_1) grows to a larger surface area then a crystal face with a faster normal growth rate (k_2); the latter diminishes in area and eventually disappears completely as shown in Figure 4.[26] In an ideal case of crystal growth, all the expected crystal faces will be present. However, the growth mechanisms are different at non-equivalent crystallographic surfaces. Consequently, smooth and rough surfaces can result from crystal growth.

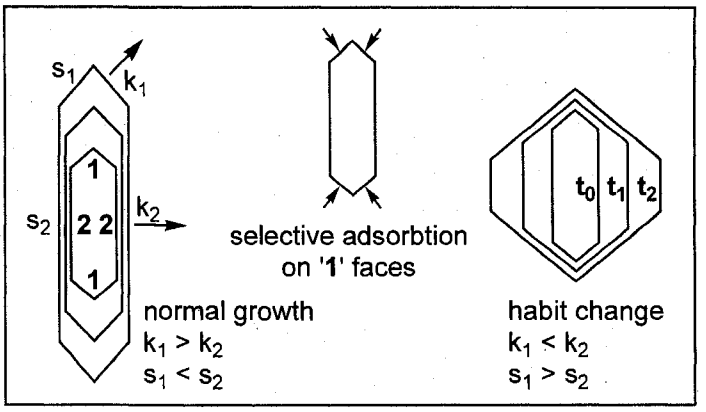

Figure 4. Relative growth rates at different crystal faces.[26] k represents the normal growth rate and t represents growth time, at a specific face S.

The Kossel crystal (Figure 5) is a simplified crystal model with different faces and the dimension of the cubes represents atomic-scale constituents (ions or molecular groups).[25] Some faces display dominantly flat surfaces (*i.e.* terraces), others show steps (*i.e.* vicinal faces such as on the edge of a $\{100\}$ face), and some atomically rough surfaces are dominated by kinks (*e.g.* at the corner of a $\{100\}$ face or on the surface of a $\{111\}$ face). As a result, two-dimensional nucleation leads to lateral growth on the crystal plane until that particular crystal surface is filled.

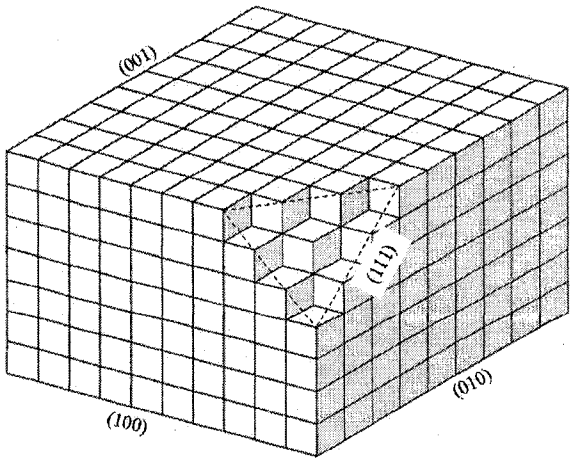

Figure 5. Kossel crystal model.[25]

1.3.4.1. Surface morphology

Growth features can be detected on surfaces at any stage of crystal growth. Depending on the roughness of the crystal faces, different characteristics of their surface topography can be observed at the nanometer scale. In general, topographic features located on flat surfaces can be formed from crystal growth or dissolution and are classified into two categories: pits and hillocks. A pit is a negative topographic feature and a hillock is a positive topographic feature. The surface topography on crystal faces can be visualized using different techniques such as phase contrast microscopy and differential interference microscopy.[25] Furthermore, features at the atomic scale can be imaged using atomic force microscopy and scanning electron microscopy.[27-29]

1.4. Historical background

Light microscopy is not suitable for visualization of atomic scale features; however, this technique combined with polarizing filters becomes a powerful tool for analyzing the rotatory power of mineral crystals. In 1811, Arago observed different colors from the polarization of incident light from a quartz plate.[20] In 1812, Biot pursued this experiment by analyzing quartz plates between a pair of polarizing filters.[30] He found that the two mirror forms of quartz crystals rotate the plane of polarized light differently. Different colors were transmitted through the quartz disk when one of the polarizing sheets was rotated clockwise or counterclockwise. Also, the angle of rotation was found to be dependent on the thickness of the quartz plate. This light transmission and polarization effect is called optical rotation.

Quartz is a classic example of a chiral terrestrial mineral crystal. Quartz (SiO_2) is not molecularly asymmetric; however, quartz crystals are macroscopically asymmetric. In the early nineteenth century Hauy identified faces on quartz that were only on alternate corners of the crystal (*i.e.* hemihedral as opposed to holohedral faces).[19] Two hemihedral forms of quartz were identified as being non-superposable mirror images of each other. It is important to note that many optically active crystals do not show hemihedral faces because the emergence of these particular faces during crystal growth (*i.e.* crystal habit) is often not favoured.[19] Important physical properties of the quartz crystal are embedded within its three-dimensional crystal structure.[31] Quartz crystals belong to the trigonal crystal system and each unit cell contains three connected tetrahedra (Z = 3). Within the quartz crystal structure, each silicon atom is attached to four oxygen atoms which form a molecular arrangement of tetrahedral SiO_4 building blocks. Since each oxygen atom is attached to two silicon atoms, the formation of a periodic tetrahedral assembly leads to an extended helical network (Figure 6).[30]

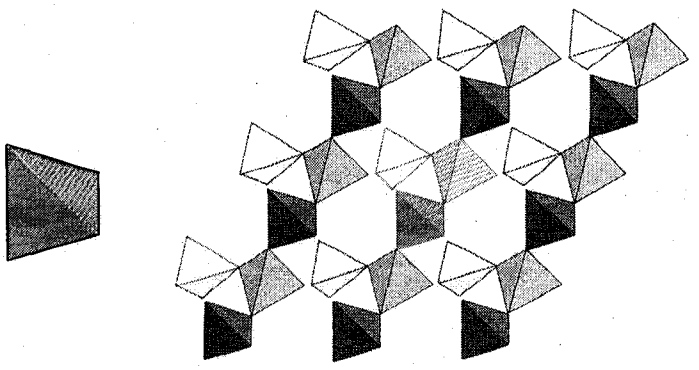

Figure 6. A tetrahedral SiO_4 building block (left) and a SiO_4 network (right).[30] Each building block consists of a silicon atom in the center with attached oxygen atoms at each corner. The three connected tetrahedra highlighted in red represent the unit cell and show the top view of a left-handed helix along the c-axis.

Quartz crystals are chiral and the chirality is determined by viewing the helical sense of the three connected tetrahedra along the c-axis. The clockwise (right-handed) helix is assigned to the chiral space group $P3_121$ and the counterclockwise (left-handed) helix is assigned to the chiral space group $P3_221$. Optical activity has been observed in isotropic, uniaxial and biaxial crystals. In isotropic crystals ORD can be observed in any crystal orientation, in uniaxial crystals ORD can only be observed along one symmetry axis of the crystal and in biaxial crystals it is harder to observe ORD because the optic axis does not coincide with any axis of crystal symmetry. Quartz crystals are uniaxial (*i.e.* anisotropic with regards to ORD).[19]

In 1848, Pasteur discovered two crystalline forms of sodium ammonium tartrate grown from a racemic solution.[32] Pasteur found that, depending on the temperature of crystallization, the formation of holohedral (>26 °C) or hemihedral (<26 °C) crystals was observed (Figure 7).[33] The holohedral crystalline form contains an equal number of left-handed and right-handed molecules in the crystal lattice (*i.e.* a cocrystal) whereas the hemihedral crystals contain only one enantiomeric form of the molecule in the crystal lattice to form either left-handed or right-handed crystals (*i.e.* conglomerates). Amazingly, Pasteur manually separated the asymmetric pairs of hemihedral crystals (crystallized from an optically inactive racemic mixture) and found that they were optically active. He concluded that dissymmetry was required for optical activity. It is important to note the difference between hemihedral crystals of sodium ammonium tartrate and chiral quartz crystals. For sodium ammonium tartrate, the chiral molecules can sometimes crystallize into two forms of enantiomorphous chiral crystals, where there is both molecular asymmetry and crystalline asymmetry. For quartz, achiral building

blocks (SiO_4) arrange in an asymmetric helical fashion to form chiral crystals, where asymmetry is absent at the molecular level but is present in the crystalline form. A nice demonstration of this phenomenon was reported in 1869 by Reusch where he created 'artificial optical activity' by stacking thin mica sheets in a helical fashion.[19]

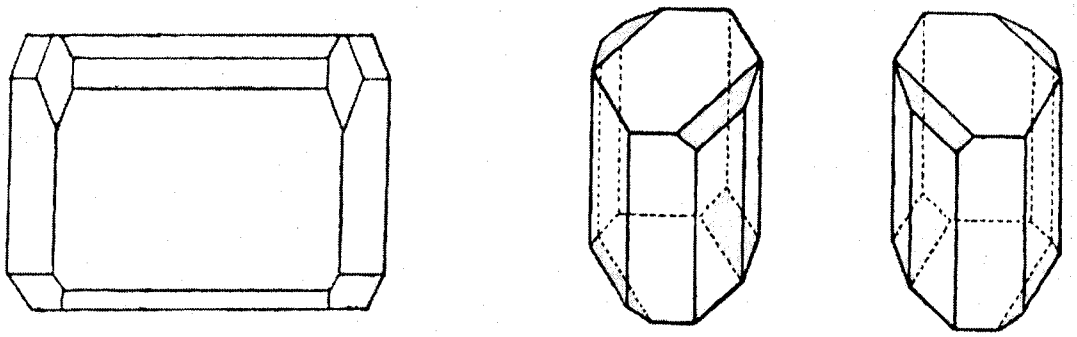

Figure 7. Holohedral crystals (left) and hemihedral crystals (right) of sodium ammonium tartrate. Hemihedral faces are shaded gray.

In brief, all chiral molecules crystallize into chiral crystals and achiral molecules can, in some cases, form chiral crystals if they crystallize in a chiral space group.

1.5. Chiral symmetry breaking and asymmetric amplification

The chirality distribution of a system (from crystallization or chemical reactions) is governed by two important processes: (*i*) chiral symmetry breaking and (*ii*) asymmetric amplification. Chiral symmetry breaking is a process which spontaneously generates an unequal mixture of enantiomers from a racemic or achiral state[34] and asymmetric amplification is a process that amplifies this initial chirality imbalance.[35] Equation 3 is introduced to calculate the percentage of a particular enantiomer in excess in a system where *R* represents the number of moles of the *R*-enantiomer and *S* represents the number of moles of the *S*-enantiomer.

$$\%\ \text{Enantiomeric Excess (EE)} = \frac{|R - S|}{R + S} \times 100 \qquad (3)$$

For chiral crystals, this equation can be modified to:

$$\%\ \text{Crystal Enantiomeric Excess (CEE)} = \frac{N_d - N_l}{N_d + N_l} \times 100 \qquad (4)$$

where N_d represents the number of *dextrorotatory* crystals and N_l represents the number of *levorotatory* crystals.

1.5.1. Chiral crystallization

Sodium chlorate ($NaClO_3$) and sodium bromate ($NaBrO_3$) are classic examples of achiral molecules that crystallize into isotropic chiral crystals. They have a unit cell of Z = 4 and crystallize in a cubic chiral space group, $P2_13$.[36] A schematic representation of chiral $NaClO_3$ crystals is shown in Figure 8.[37]

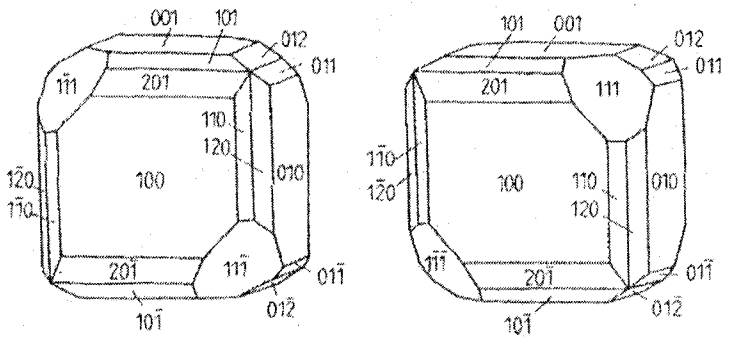

Figure 8. Schematic representation of a *levorotatory* (left) and *dextrorotatory* (right) sodium chlorate crystal.[37]

Spontaneous crystallization of these inorganic salts is expected to give an equal amount of both enantiomorphic crystals because both enantiomers have identical stability and

equal probability to nucleate and grow. Some more examples of achiral compounds forming chiral crystals are listed in Table 2.[19, 38]

Table 2. Examples of achiral compounds forming chiral crystals.[19, 38]

Isotropic	Uniaxial	Biaxial
Sodium chlorate	Quartz	Hydrazine sulfate
Sodium bromate	Cinnabar	Strontium formate
Sodium sulfantimoniate	Sodium periodate	Barium formate
Sodium uranyl acetate	Potassium dithionate	Lead formate
	Rubidium dithionate	Iodic acid
	Cesium dithionate	Ammonium oxalate
	Calcium dithionate	Ammonium potassium oxalate
	Strontium dithionate	Sodium arsenate
	Lead dithionate	Lithium sulphate
	Ethylenediamine sulfate	Magnesium sulphate
	Benzil	Nickel sulphate
	Potassium lithium sulfate	Magnesium chromate
	Potassium lithium sulfochromate	Sodium dihydrogen phosphate
	Guanidine carbonate	
	Diacetylphenolphthalein	
	Potassium silicomolybdate	
	Potassium silicotungstate	

In 1898, Kipping and Pope performed chiral crystallization experiments with sodium chlorate in solution.[39] In one set of experiments, 3137 crystals were collected and the chirality of these crystals was analyzed under a polarizing microscope. A statistically equal number of *dextrorotatory* and *levorotatory* crystals was obtained (1571 *dextrorotatory* crystals: 1566 *levorotatory* crystals) from primary nucleation events.

1.5.2. Stirred crystallization

In 1990, Kondepudi *et al.* demonstrated that the mirror symmetry of sodium chlorate crystals can be broken when the crystallization is carried out with constant stirring.[40] The experiment was performed by stirring an unsaturated sodium chlorate solution (25 mL) in a 100 mL beaker at *ca.* 100 rpm using a Teflon magnetic stir bar (4 mm x 4 mm). The beaker was covered with tissue paper to avoid external contamination and the chirality of the grown crystals was analyzed between polarizing filters. Thirty-two stirred crystallization experiments were performed and a total of 11829 crystals were analyzed; 18 experiments showed a dominating population of *dextrorotatory* crystals and 14 experiments showed a dominating population of *levorotatory* crystals. In 1993, 60 stirred crystallizations were performed and the effect of stirring on the spontaneous crystallization clearly showed a bimodal distribution of the two enantiomorphic populations of $NaClO_3$ crystals.[41] The distribution of CEE for unstirred crystallizations (chiral crystallization) was centered at zero whereas for stirred crystallization, the distribution peaks for *d* and *l* crystals were concentrated at 1.0 and -1.0 (or 100% and -100% if expressed as a percentage according to equation 4).

This spontaneous chiral symmetry breaking process is caused by rapid secondary nucleation where the first (and only) crystal from primary nucleation is broken down into smaller pieces due to stirring. These smaller daughter crystals all possess the same chirality as the initial mother crystal in the system and become the new nucleation sites for crystal growth. Consequently, the resulting crystals are homochiral. In theory, the decrease in solution concentration due to secondary nucleation will suppress other primary nucleation events to occur. This secondary nucleation is also called a nonlinear

autocatalytic process.[42] This chiral symmetry breaking method is called *stirred crystallization*.

An example of an organic compound that can be crystallized from the melt into a tetragonal chiral space group, $P42_12_1$, is 1,1'-binaphthyl (Figure 9).[43] Unstirred chiral crystallization of 1,1'-binaphthyl at 150 °C gave optically inactive crystals (a conglomerate racemic mixture of both *R*-(–) and *S*-(+) crystals) as expected from primary nucleation.[44]

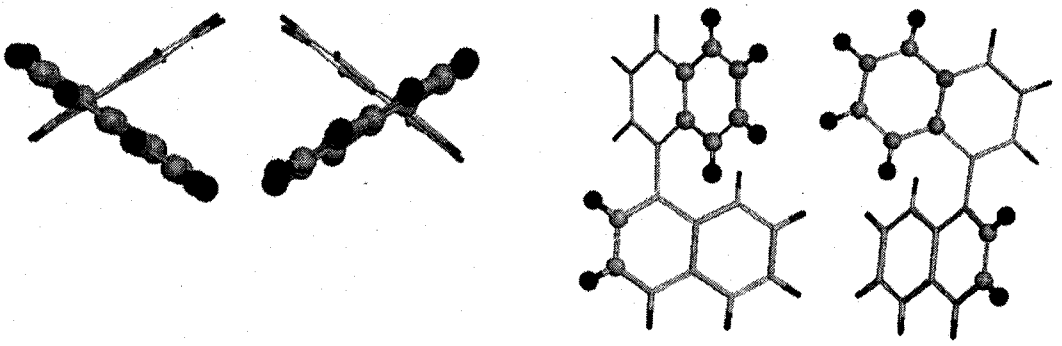

Side view Front view

Figure 9. Ball-and-stick models of 1,1'-binaphthyl. Side view (left) and front view (right) of enantiomeric 1,1'-binaphthyl molecules.[43]

In 1999, the chiral symmetry breaking of 1,1'-binaphthyl was achieved by stirring a melt sample at 180 °C which was slowly cooled to 150 °C.[45] As a result, a large enantiomeric excess (*ca.* 77% EE) of *R*-(–) or *S*-(+) crystals was produced due to secondary nucleation.

The complete chiral symmetry breaking of a racemic system requires an amplification of the enantiomer in excess *and* the depletion of the minor enantiomer until homochirality is reached.

1.5.3. Abrasion/grinding technique

The chiral symmetry breaking of $NaClO_3$ from a racemic mixture was achieved by Viedma using an abrasion/grinding technique.[46] A racemic mixture of *d* and *l* $NaClO_3$ crystals (ground with a mortar and pestle) was stirred at 600 rpm in the presence of 3 mm diameter glass beads in a saturated solution in a sealed flask. The resulting crystalline seeds were sampled every 6 hours and were allowed to grow until large enough for examining chirality of the grown crystals using a polarizing microscope. The percentage CEE of the sample was calculated according to equation 4. After 24 hours of abrasion/grinding, the CEE of the closed system reached 100%.[47] The amount of grinding media and the stirring rate were found to be closely related to the time required for achieving enantiopure crystals; as the relative amount of glass beads and the stirring rate increased the time required to reach homochirality decreased.[46] More importantly, the chirality of the enantiopure crystals can be directed by incorporating an initial imbalance in the starting mixture. For example, the addition of a 5% CEE of *d*-$NaClO_3$ crystals directed the chiral symmetry breaking towards 100% CEE of *d* crystals; whereas the addition of a 5% CEE of *l*-$NaClO_3$ crystals directed the chiral symmetry breaking towards 100% CEE of *l* crystals.[46] Recently, chiral symmetry breaking of $NaClO_3$ was also achieved by applying an ultrasonic field to a supersaturated solution and a CEE of over 90% was obtained in most cases.[48]

Viedma proposed that the mirror symmetry breaking process is governed by two mechanisms: (*i*) Ostwald ripening and (*ii*) a recycling process. According to the Ostwald ripening principle, large crystals grow at the expense of smaller crystals.[49] The small crystals possess a larger surface to volume ratio than the large crystals and therefore the

smaller crystals are thermodynamically less stable and are more readily dissolved. Crystal dissolution of the smaller crystals creates a concentration gradient. This difference in solute concentration becomes the driving force for the achiral molecules to move from smaller crystals to larger crystals. According to Viedma, the recycling process is responsible for the amplification of the initial enantiomeric excess and the depletion of the minor enantiomer in the system. This process is also known as the common ancestor effect where, 'the removal of competing lineages leaves just one common ancestor for the entire system'.[49] The abrasion/grinding technique developed by Viedma that leads to homochirality is illustrated in Figure 10.[50] It is important to note that the depletion of the enantiomer in minority will not occur if the chiral symmetry breaking process is governed solely by secondary nucleation.

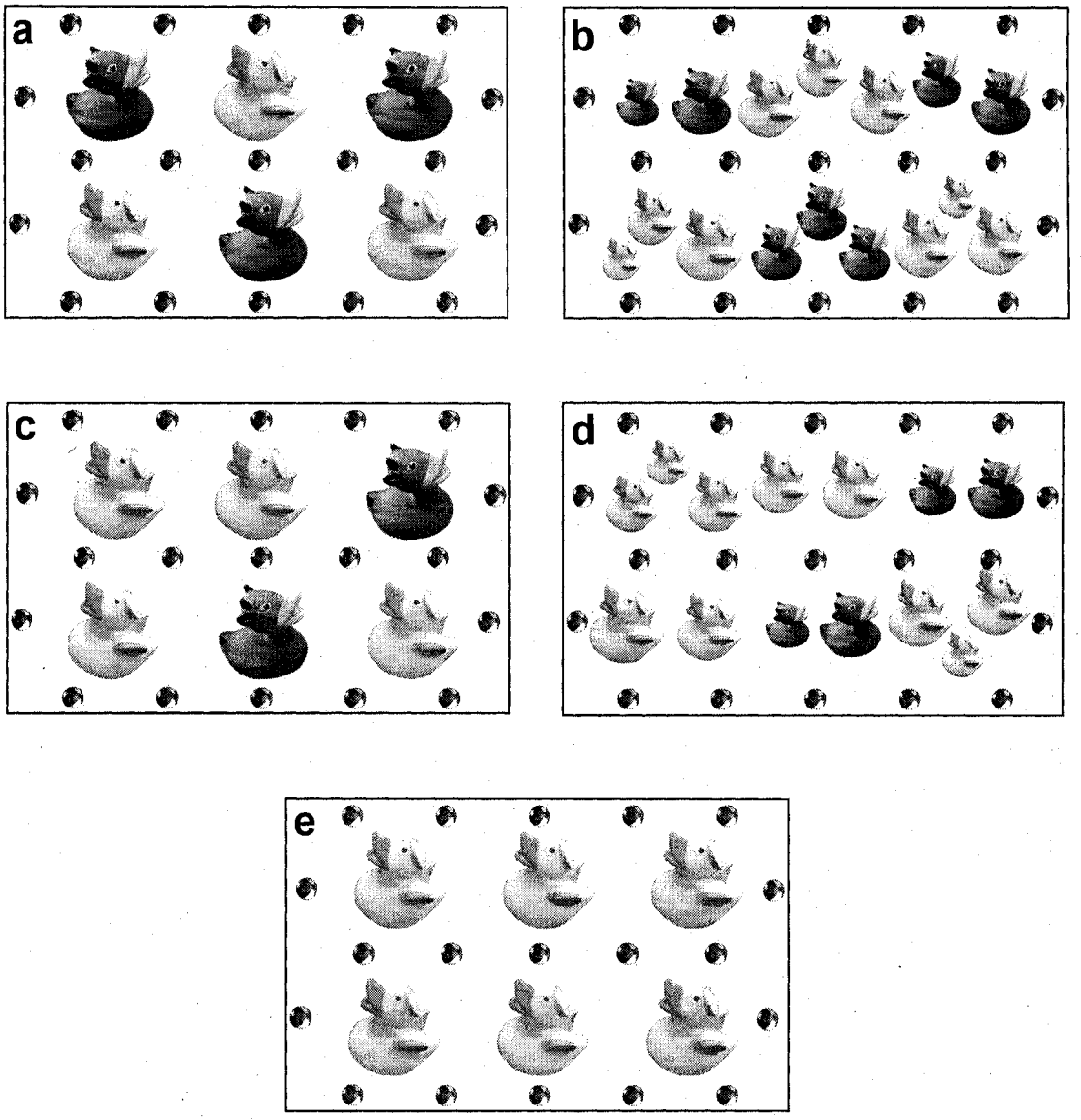

Figure 10. Simplified cartoon representation of the abrasion/grinding technique (a modified version of Viedma's model).[50] The red devil ducks represent *dextrorotatory* crystals, the white angel ducks represent *levorotatory* crystals, and the beach balls represent grinding media. (a) Starting with a racemic mixture of 50% *dextrorotatory* and 50% *levorotatory* crystals in saturated solution in the presence of grinding media, the crystalline surfaces experience continuous dissolution and recrystallization. (b) Under constant stirring, the chiral crystals are broken down into smaller crystals of the same chirality. These smaller crystals dissolve more easily into achiral molecules. (c) Subsequently, the achiral molecules feed growing crystals in the system independently of their chirality during Ostwald ripening. In this case the white angel ducks represent the dominant chirality among the growing crystals. (d) As the recycling process continues, the number of white angel ducks (chirality in dominance) amplifies. (e) Homochirality with 100% white angel ducks is eventually obtained.

1.5.3.1. Chiral impurities/additives

Viedma further pursued the chiral symmetry breaking of $NaClO_3$ and $NaBrO_3$ using the abrasion/grinding method and found that a high CEE of *l*-crystals, up to 99%, was obtained for both cases.[51] This preference of *l*-crystals is believed to be due to the presence of chiral impurities from the environment (also called cryptochiral impurities) and creates an initial bias in the racemic system which is further amplified during the recycling process. Interestingly, an example of enantioselectivity during crystal growth of $NaClO_3$ and $NaBrO_3$ was reported in 1972.[52] The addition of *d*- or *l*-$NaBrO_3$ crystalline seeds in a $NaClO_3$ supersaturated solution induced the growth of $NaClO_3$ crystals with the opposite chirality. The same effect was observed with the addition of chiral $NaClO_3$ crystalline seeds in a $NaBrO_3$ saturated solution.[53] Moreover, Niedermaier and Schlenk Jr. demonstrated the influence of chiral additives during crystal growth.[52] For example, the CEE of *d*-$NaClO_3$ crystals increased to homochirality in the presence of D-mannitol; whereas the CEE of *l*-$NaClO_3$ crystals increased to 98% in the presence of D-sorbitol. In the case of $NaBrO_3$, the CEE of *l*-crystals increased to 93% in the presence of D-mannitol; whereas the CEE of *d*-crystals increased to homochirality in the presence of D-sorbitol. In addition, the symmetry of supramolecular chiral assemblies of achiral molecules can also be influenced by the presence of chiral initiators.[54, 55]

1.5.3.2. Etch figures

Microtopographical evidence of molecular adsorption on $NaClO_3$ crystal surfaces was obtained by observing the etch figures after exposure to an etchant. For example, the addition of formic acid on the $\{100\}$ faces of a *d*- and *l*-$NaClO_3$ crystal led to the

formation of mirror-related elongated parallelogram-shaped etch pits (Figure 11).[56] In the presence of etchant, it is believed that the geometric shape of the etch figures is affected by the dissolution rate on specific crystalline faces.

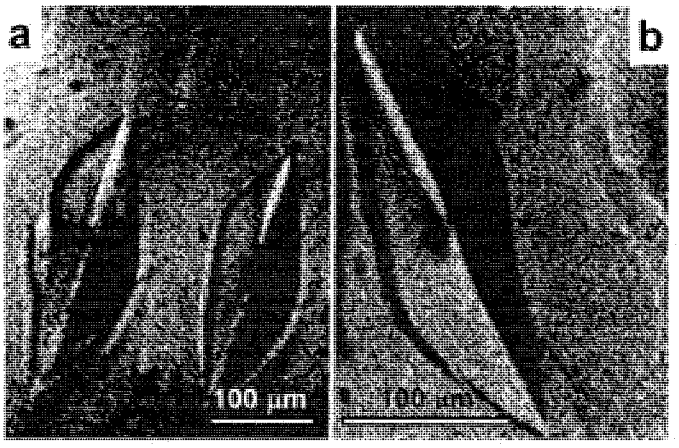

l-sodium chlorate *d*-sodium chlorate

Figure 11. Etch figures on $\{100\}$ faces of (left) *l*- and *d*-sodium chlorate crystal.

1.5.4. Enantioselective adsorption

In addition to inorganic salts, a wide range of terrestrial minerals have been investigated to provide valuable information of chiral molecular recognition on crystal surfaces.[57] These mineral surfaces are believed to be a possible platform for self-assembly of biomolecules into more complex structures.[58] Chiral amino acids are often used as chiral agents for asymmetric adsorption experiments because of their chirality preference in nature.

1.5.4.1. Terrestrial minerals

Quartz is one of the classic examples of a chiral crystal used in asymmetric adsorption studies. A slight imbalance in favour of the *l*-form of quartz is observed in nature (1.4% excess of *l*-quartz among 16807 samples collected worldwide).[31] An

experimental study showed that radioactive D-alanine preferentially adsorbs on a powdered *d*-quartz sample; whereas radioactive L-alanine preferentially adsorbs on a powdered *l*-quartz sample.[12]

Another kind of terrestrial mineral, calcite ($CaCO_3$), was abundant in the Archean period when earth's atmosphere was hot and contained little oxygen and other gases that are not suitable for living organisms.[59] An analogue of a calcite crystal at the molecular level is a meso compound. Meso compounds have more than one chiral center but possess a plane of symmetry so they are overall achiral. Similarly calcite crystals are overall achiral but possess mirror-related faces. The trigonal scalenohedral crystal form is often chosen for chiral selectivity studies because of these adjacent mirror-related faces (Figure 12).[13]

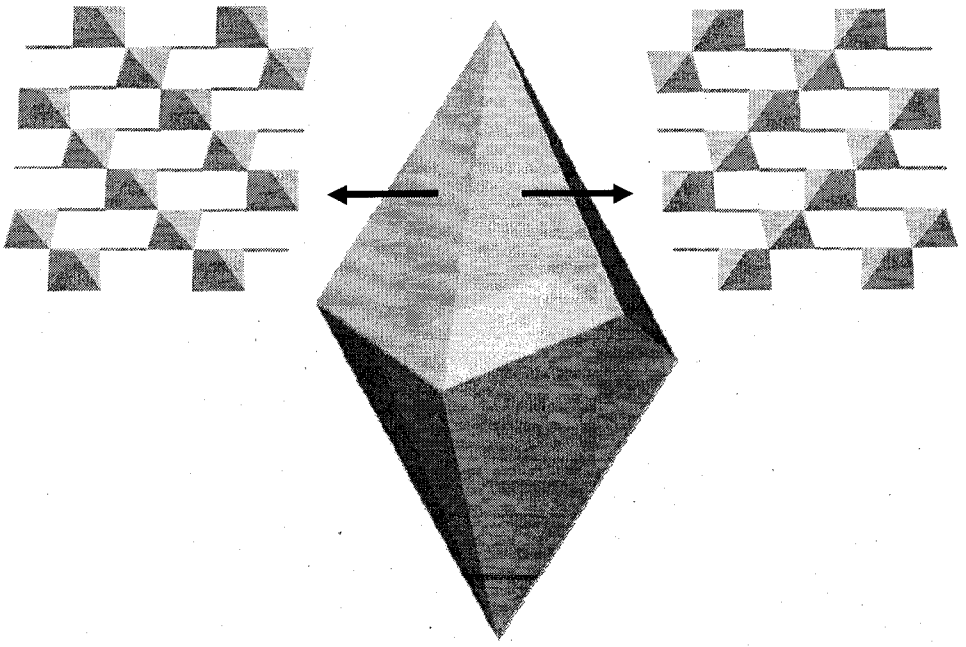

Figure 12. Schematic representation of adjacent mirror-related faces of a $CaCO_3$ crystal.[13, 31] The asymmetric crystal surface is composed of CaO_6 octahedra chains that are connected through planar CO_3 groups (shown as horizontal lines).

The chiral selectivity experiment was performed by immersing scalenohedral calcite into a racemic aspartic acid solution (0.05 M) for 24 hours. The adsorbed amino acid was removed by pipetting HCl (0.02 M) on individual crystal surfaces (right hand or left hand) for 20 seconds, the acid wash was collected in the same pipette and this procedure was repeated three times on three successive days. The collected aspartic acid samples were analyzed using gas chromatography. The ratio of D- versus L-aspartic acid showed that the right hand faces preferentially adsorbed D-aspartic acid whereas the left hand faces preferentially adsorbed L-aspartic acid. Furthermore, asymmetric adsorption can influence the morphology of a chiral crystal surface. The growth of rhombohedral calcite crystals in a supersaturated solution in the presence of a chiral solute showed changes in the geometric shape of the growth hillocks on the $\{104\}$ faces using atomic force microscopy (AFM).[29] The growth hillocks of a calcite crystal without chiral additive show straight step edges; however, the presence of 0.01 M D- or L-aspartic acid modified the straight step edges into rounded growth hillocks (Figure 13).[60]

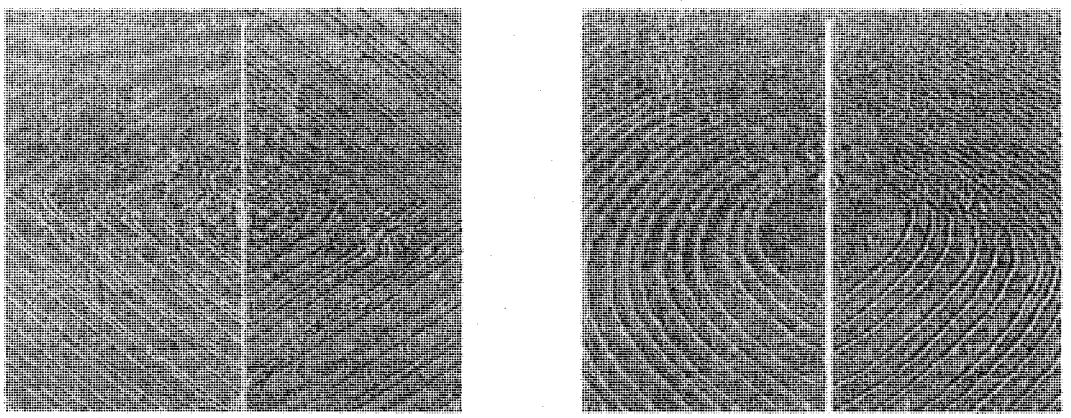

Figure 13. Liquid-immersion AFM images of growth hillocks on a cleaved $CaCO_3$ crystal surface.[60] In the absence of chiral aspartic acid (left), and in the presence of chiral aspartic acid (right).

Aspartic acid in the supersaturated solution is believed to behave as a growth inhibitor and therefore modify the shape of the growth hillocks in an enantioselective fashion. Under unsaturated conditions and in the presence of chiral aspartic acid, asymmetric etch pits were observed on the calcite crystal surface and the edges were inclined at a different angle relative to the edges in the presence of the D- or L-aspartic acid (Figure 14).[29] The symmetrically related etch figures on different chiral crystals is believed to be due to different dissolution rates at specific chiral crystal faces.

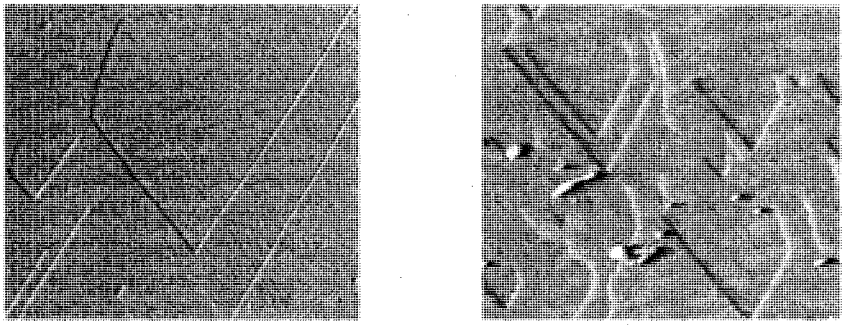

L-aspartic acid D-aspartic acid

Figure 14. AFM images of etch pits on chiral $CaCO_3$ crystal surfaces.[29] Both crystals are orientated in the same direction. 10 x 10 μm size image in the presence of L-aspartic acid (right) and 5 x 5 μm size image in the presence of D-aspartic acid (left).

Gypsum ($CaSO_4 \cdot 2H_2O$) is another example of a natural terrestrial mineral possessing chiral faces which exhibits selective adsorption of chiral molecules on chiral faces. In the absence of chiral additive, gypsum grows into bilaterally symmetrical crystals, but its crystal habit can be influenced by the adsorption of chiral amino acids on selective faces during crystal growth.[14] For example, crystal faces on opposite sides of the mirror plane of symmetry in gypsum have an unequal affinity for the enantiomers of glutamic acid, alanine and arginine.

These morphological changes due to enantioselective adsorption on crystal surfaces is shown in Figure 4.[61] Under normal growth conditions, the relative growth rate (k_1) of surface 1 is faster than the relative growth rate (k_2) of surface 2. As mentioned previously, slower growth rates will lead to a larger surface area and therefore surface 2 (S_2) becomes larger than surface 1 (S_1). If selective adsorption of a chiral molecule occurs at surface 1, the crystal growth at surface 1 is inhibited and therefore results in a slower growth rate relative to that of surface 2. As the crystal grows to a larger size in the presence of a chiral additive, the surface area of 1 becomes bigger and that of 2 becomes smaller and may eventually disappear. This change of growth rate leads to macroscopic habit modifications as observed in gypsum.

1.5.4.2. Inorganic crystals

Evidence for the enantioselective adsorption of chiral molecules on chiral crystals requires an amplification process (as described for $NaClO_3$) or topological feature analysis (*e.g.* growth hillocks and etch figures). Indeed, dye molecules were found to be selectively adsorbed onto specific crystal faces and were employed as a visualization tool to display the adsorption area of crystal growth. As a result, the crystal habit modification due to dye inclusion often leads to an hourglass (bow-tie shape) pattern. These dye inclusion crystals (DICs) are grown in solution in the presence of an organic dye.[62, 63] Potassium dihydrogen phosphate (KH_2PO_4) and potassium sulfate (K_2SO_4) are two of the classic examples of ionic salts that form DICs. The incorporation of dye molecules, such as Chicago sky blue (a blue dye) or amaranth (a red dye), at the $\{101\}$ growth sectors during the crystal growth of KH_2PO_4 led to the formation of DICs with blue or red 'bow-tie' patterns as shown in Figure 15.[63, 64]

Figure 15. Dye inclusion of KH_2PO_4 crystal with amaranth.

The preferential inclusion of these anionic dyes at selective faces is believed to be due to the ionic interactions with the exposed K^+ ions at the adsorption faces.[65] The growth rate of the adsorption crystal faces was slowed down and led to a larger dyed area as described previously in Figure 4.[61] The hourglass inclusion effects also occurred during the growth of K_2SO_4 crystals in the presence of acid fuchsin (a pink dye) at the $\{110\}$ growth sectors.[66] In addition, two dyes (acid fuchsin and naphthol green B) can be incorporated into the $\{110\}$ and $\{001\}$ growth sectors, respectively, in the same K_2SO_4 crystal (Figure 16).[64, 67]

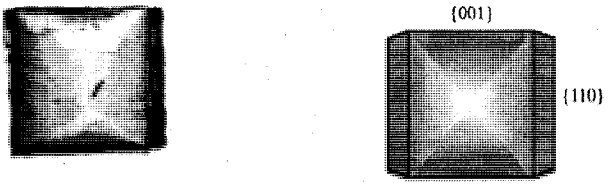

Figure 16. Dye inclusion K_2SO_4 crystal with acid fuchsin and naphthol green B. [64, 67] 4 x 4 x 1 mm^3 size crystal (left) and a schematic representation of dye inclusion at the $\{001\}$ and $\{110\}$ growth sectors (right).

More importantly, crystal dying was also found to be useful for separating chiral crystals. In the presence of yellow N^{ε}-(2,4-dinitrophenyl)-(*S*)-lysine during the crystal growth of glutamic acid·HCl, the *R*-enantiomer was first precipitated as colorless crystals followed by the growth of larger yellow crystals of the *S*-enantiomer.[26]

In brief, crystal growth in the presence of dye additives can provide information on molecular adsorption sites and enantiomeric resolution.

1.5.5. Asymmetric synthesis

Asymmetric amplification due to the presence of impurities or additives is an important aspect in crystallization and in enantioselective organic synthesis.

1.5.5.1. Absolute asymmetric synthesis using chiral crystals

Absolute asymmetric synthesis is well-known to benefit pharmaceutical industries in producing the enantiomeric form of the molecule of interest with high yield.[68] Asymmetric synthesis of enantioenriched molecules can be induced by the addition of a chiral agent. An example is the nucleophilic carbonyl addition of *n*-butyllithium using chiral crystals of *N,N*-disubstituted 2-benzoylbenzamides (achiral molecules that crystallize in the chiral space group, $P2_12_12_1$).[69] The powdered form of the chiral crystals was incorporated into the reaction mixture as a chiral catalyst and the desired product was obtained in over 80% yield with an enantiomeric excess as high as 84%.

1.5.5.2. Asymmetric autocatalytic synthesis

Another method of asymmetric amplification developed by Soai and coworkers uses the enantioenriched product of a reaction as a chiral catalyst (*i.e.* autocatalysis). A well known example is the enantioselective alkylation of pyrimidine-5-carboxylaldehyde using diisopropylzinc (Figure 17).[70] A small amount (with EE as low as 2%) of the chiral product (*i.e.* the catalyst), *S*-2-methyl-1-(5-pyrimidyl)propan-1-ol, was introduced back into the reaction mixture and following the addition of the starting reagents the

production of a significant amount of the same chiral product was obtained with an EE as high as 89% after four cycles.

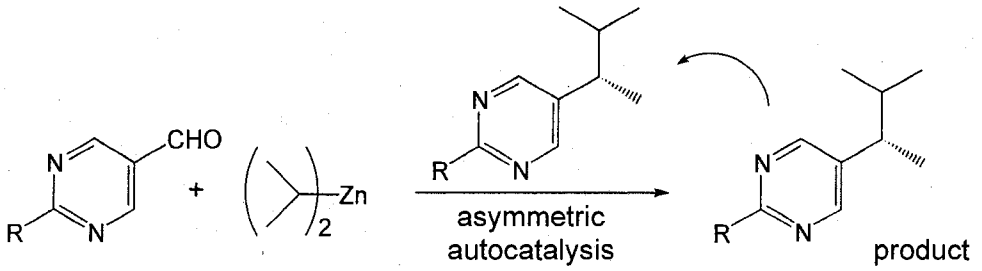

Figure 17. Asymmetric autocatalytic alkylation of pyrimidine-5-carboxylaldehyde using diisopropylzinc. The chiral product acts as a chiral catalyst for its own production.[70]

Interestingly, the Soai autocatalytic reaction can be triggered by other chiral initiators. For example, the addition of D- or L-leucine (*ca.* 2% EE; obtained from photolysis of a racemic leucine sample using right or left-CPL)[71] led to the formation of the *S*-alkylated product (26% EE) and the *R*-alkylated product (23% EE), respectively.[72] Asymmetric autocatalysis can also be performed in the presence of chiral crystals such as quartz. The Soai reaction was carried out by adding powdered *d*- or *l*-quartz crystals (μm size) to the reaction mixture at 0 °C and yielded high EE of *S*- and *R*-2-(*tert*-butylethynyl)-5-pyrimidyl alkanol, respectively.[73]

The influence of chiral sodium chlorate or sodium bromate crystals on the Soai reaction was also explored. The incorporation of powdered *d*-$NaClO_3$ crystals led to a high EE of *S*-2-(*tert*-butylethynyl)-5-pyrimidyl alkanol whereas the incorporation of powdered *l*-$NaClO_3$ crystals led to a high EE of the *R*-enantiomer.[74] On the other hand, when $NaBrO_3$ crystals were used, the presence of *d*-crystals yielded high EE of the *R*-product whereas the presence of *l*-crystals yielded high EE of the *S*-product.[75] Finally, the enantioselectivity of the Soai reaction can also be influenced by exposure to CPL (*ca.*

300 nm) in vacuum prior to asymmetric autocatalysis.[76] The irradiation of a racemic sample of 2-(*tert*-butylethynyl)-5-pyrimidyl alkanol with right-CPL induced the production of cryptochiral *R*-enantiomer and the irradiation of the racemic sample with left-CPL induced the production of cryptochiral *S*-enantiomer. These chiral pyrimidyl alkanols were used as catalysts for the enantioselective synthesis of 2-(*tert*-butylethynyl)-pyrimidine-5-carbaldehyde. The addition of the *R*-enantiomer amplified the synthesis of the *R*-product and the addition of the *S*-enantiomer amplified the synthesis of the *S*-product.

1.5.6. Phase behaviour models of chiral amplification

To illustrate the enantiomeric amplification process of a non-racemic system becoming enantiopure, phase behaviour models have been established to represent the solid-liquid equilibrium in a simplified manner.

1.5.6.1. 'Chiral amnesia' in the solid phase

Recently, a new term, 'chiral amnesia', was introduced to describe the establishment of homochirality in the solid phase from an achiral or a chiral system (Figure 18).[77] Under saturated conditions, achiral molecules (A) can be crystallized into an equal amount of conglomerates (A_D and A_L). Continuous dissolution and recrystallization takes place on crystal surfaces at solid-liquid equilibrium and the chirality of the solid phase is not preserved during this process. As a result, the achiral molecules (A) from dissolution will recrystallize into either chirality. This model correlates perfectly with Viedma's model of chiral symmetry breaking of $NaClO_3$ using an abrasion/grinding method.[46] Similarly, chiral molecules can be crystallized into

conglomerates (D and L). In this case, the chiral molecules from dissolution undergo rapid racemization to maintain an equal amount of D and L molecules in the solution phase. However, D molecules will only be recrystallized into D solid whereas, in this case, L molecules will only be recrystallized into L solid. The chirality of both enantiomers is preserved during the dissolution and recrystallization process. The solubility is doubled in the solution phase due to the independent solid-liquid equilibrium of D and L enantiomers with its own species. This phenomenon is also called the 'Meyerhoffer double solubility rule'.[78]

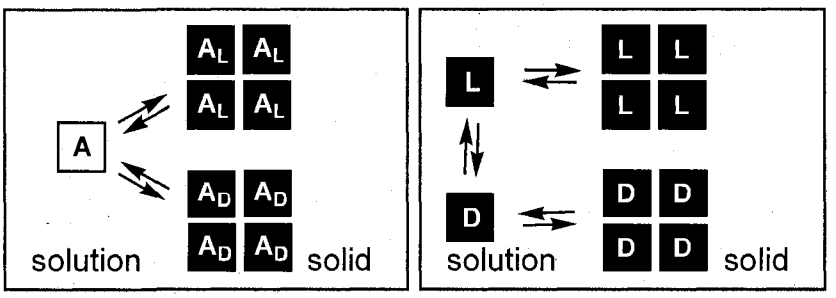

Figure 18. Schematic representation of the solid-liquid equilibrium in the solid phase. An achiral molecule that crystallizes into enantiomorphic solids (left) and a chiral molecule that crystallizes into conglomerates (right).

Recently, this was demonstrated experimentally by stirring a racemizing sample of *N*-(2-methylbenzylidene)-phenylglycine amide with the addition of 3 – 10% EE of its *R*- or *S*-crystals in the presence of grinding media.[79] The EE obtained showed that the chirality of the resulting enantiopure sample depends on the initial enantioimbalance established in the racemizing mixture. The addition of *S*-phenylglycine or *R*-phenylglycine in the sample mixture led to the formation of homochiral *R*- and *S*-*N*-(2-methylbenzylidene)-phenylglycine amide, respectively. As discussed previously, the *R* crystals dissolve into *R* molecules in the solution phase which racemize with the *S*

molecules resulting from *S* crystal dissolution. The addition of a chiral agent shifted the racemization process in the solution phase to favour one of the enantiomers and subsequently the solubility of the *R* or *S* enantiomer in the solid phase. This chirality bias was amplified during the solid-liquid equilibrium and led to 'chiral amnesia'. Concisely, the solubility difference of enantiomers in solution plays an important role in achieving homochirality under solid-liquid equilibrium conditions.

1.5.6.2. 'Chiral amnesia' in the solution phase

Besides the establishment of enantiopurity in the solid phase, similar asymmetric amplification effects can be observed in the solution phase. The characteristic solubility of a mixture of components in the solution phase at a fixed temperature is described as the eutectic.[38] Threonine is an example of a chiral molecule that forms D and L crystals and exhibits 0% eutectic EE in the presence of an unequal amount of both enantiomers under equilibrium conditions in water at 25 °C.[80] In this case, both amino acid conglomerates are equally soluble under equilibrium conditions and therefore a 0% eutectic EE is observed (Figure 19).[81] The eutectic EE in solution is based on the solubility of the conglomerates and not the amount of D or L solid present in the solution phase. As long as both enantiomers are equally soluble, the eutectic EE will be zero.

The eutectic EE can be amplified when a chiral molecule crystallizes into heterochiral DL solid and a slight excess of one enantiomer is present in the solution phase (Figure 19). This asymmetric amplification was observed for serine when its heterochiral DL solid and a slight excess of the L-enantiomer were present in water at 25 °C under equilibrium conditions.[80, 82] A high eutectic EE of >99% was obtained because of the solubility

difference between heterochiral DL solid and homochiral L solid in the solution phase.[81] In this case, the DL solid is much less soluble compared to the L solid and therefore a high eutectic EE was observed in the solution phase. The fact that serine preferentially crystallizes into DL solid rather than homochiral solid shows that the intracrystalline interactions of a DL solid is stronger than that of a homochiral solid. As a result, the DL solid is less soluble than the homochiral D or L solid.[81, 82]

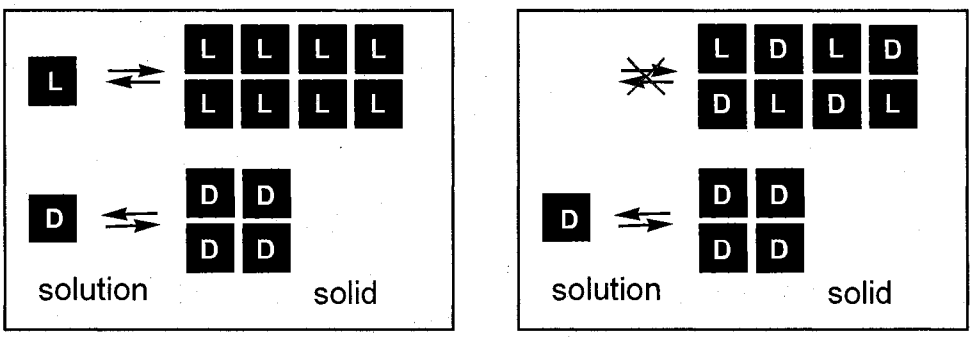

Figure 19. Schematic representation of the solid-liquid equilibrium in the solution phase. Conglomerates with 0% eutectic EE (left) and asymmetric amplification of a racemic compound (1:1 ratio of the D and L enantiomer in the solid) in the presence of an enantiomeric excess in the solution phase under solid-liquid equilibrium conditions with a eutectic EE greater than 0% (right).

Blackmond strongly believes that chiral symmetry breaking and asymmetric amplification processes are the essential criteria that lead to 'chiral amnesia'.[77]

1.5.6.3. 'Chiral amnesia' in the gas phase

Chiral amplification can also be achieved in the gas phase through sublimation. Studies of the amplification of an initial enantioimbalance of different amino acid samples have been performed at high temperature and a high percent enantiomeric excess was found in the resulting sublimates. Cooks and coworkers studied the sublimation of serine racemate in the presence of L-serine (3 – 75% EE) in the temperature range of

175 – 230 °C and the composition of the thermolysis products showed a high EE of L-serine (68 – 99%).[83] Feringa and coworkers also demonstrated similar enrichment of several amino acid racemates (leucine, phenylalanine, alanine, valine, methionine and serine) with slight initial enantioimbalance (0.5 – 10 % EE of the L-enantiomer) through sublimation in the temperature range of 90 – 270 °C.[84] The percentage enantiomeric excess of the L-amino acids in the sublimate was amplified up to 89%. The enantioenrichement of amino acids through sublimation is believed to be due to the different volatility between amino acid racemates and pure enantiomers.[81, 84] The intermolecular interactions in these racemates are stronger than that of pure amino acid enantiomers. Consequently, the racemates sublime more slowly compared to the enantiopure amino acids resulting in higher EE of the faster sublimating species in the gas phase. In brief, homochirogenesis can occur in the solid, liquid or gas phase.

1.6. Statement of objective

The objective of this project is to investigate the chiral crystallization, mirror symmetry breaking and asymmetric amplification of ethylenediammonium sulfate (EDS), an achiral molecule that crystallizes into chiral crystals. Mirror symmetry breaking and chiral amplification were achieved using an abrasion/grinding technique in the absence or presence of chiral amino acids. This study provides useful information on enantioselective adsorption of chiral biological molecules on chiral mineral surfaces. Based on the possible mechanisms proposed for chiral selection, the enantioselective adsorption on ethylenediammonium sulfate crystals may give insight for understanding homochirogenesis in nature.

1.7. Ethylenediammonium sulfate (EDS)

Ethylenediammonium sulfate (EDS) is an achiral molecule that crystallizes into the tetragonal chiral space group, $P4_1$.[85] The optical rotation of EDS was first reported by Groth in 1910 to be 15.5° mm^{-1} (sodium D line).[86] The ethylenediammonium cation adopts a chiral gauche conformation resulting in an overall helical arrangement of the $[H_3NCH_2CH_2NH_3]^{2+}$ and $[SO_4]^{2-}$ ions (Figure 20) in a unit cell of 5.993 Å, 5.993 Å, and 18.047 Å for the a-, b-, and c-axes, respectively.[85]

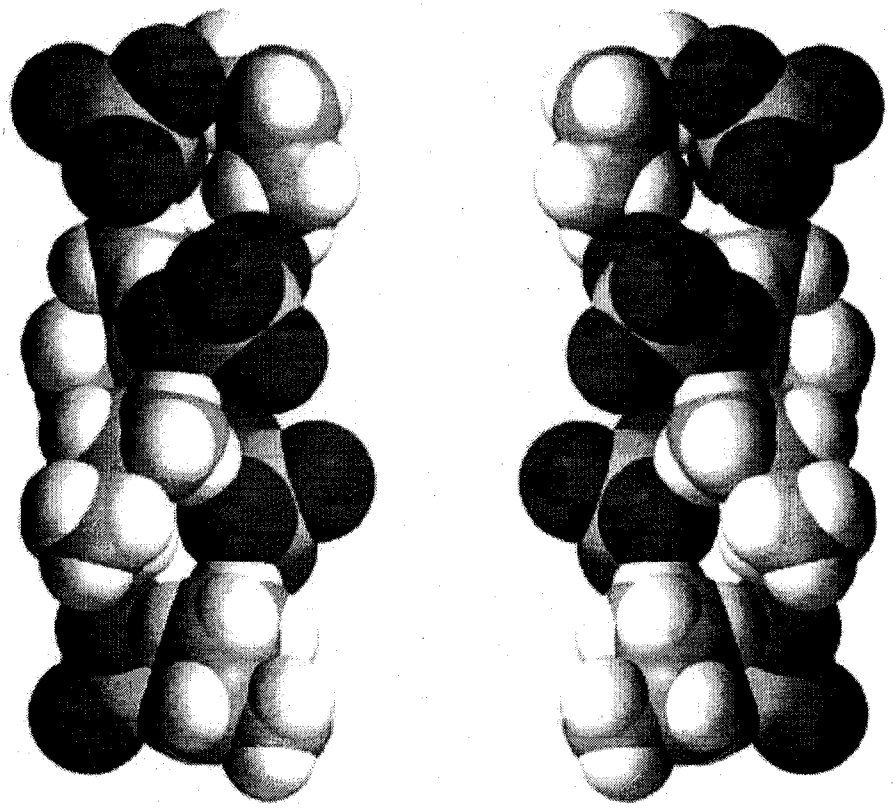

Figure 20. An enantiomeric pair of helical EDS unit cells.[85]

The resulting tetragonal crystals are anisotropic and the optical rotatory dispersion can be visualized through the (001) and $(00\bar{1})$ face using a polarizing microscope (Figure 21).

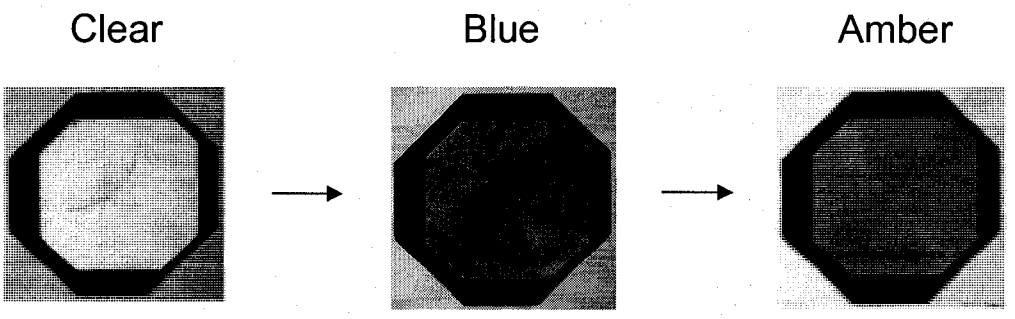

Figure 21. Optical rotatory dispersion of a *dextrorotatory* EDS crystal. The color changes from clear to blue to amber when the analyzer is rotated clockwise.

Chapter 2. Experimental

'Oh, you're not Piglet,' he said. 'I know Piglet well, and he's *quite* a different color.'

Winnie-the-Pooh
A.A. Milne

2.1. Materials and methods

Ethylenediamine [CAS 107-15-3] (certified anhydrous; $NH_2CH_2CH_2NH_2$; F.W. 60.10) was purchased from Fischer Scientific and sulfuric acid [CAS 7664-93-9] (96.8%; 18.2 M; A.C.S. reagent; H_2SO_4; F.W. 98.08) was purchased from J.T. Baker. Ethylenediammonium sulfate [CAS 25723-52-8] was synthesized as described in section 2.1.1.

Deionized water was used for unsaturated and saturated solution preparation and the pH was verified using pH paper (pHydrion, INSTA-CHEK 0 – 13, Micro Essential Laboratory, Brooklyn, N.Y. U.S.A.). The resulting saturated solution was centrifuged at speed level 4 (International Clinical Centrifuge; model CL; International Equipment Co.) using 50 mL plastic centrifuge tubes (Falcon or SARSTEDT) prior to use for crystalline seeding. Growth of crystalline seeds was performed in crystallizing dishes purchased from Kimax (No. 23000; 100 x 50). Tweezers with pointed ends (stainless, antimagnetic, anti acid; Model 3CSA) were purchased from *technik* and were used for collecting EDS crystal samples and individual EDS crystals were dried using Kimwipes (KIMTECH Science, 11 cm x 21 cm).

The stirring rate of commercial stirrers was verified using a strobe light (Strobotac Stroboscope, type 1538A, General Radio Co., Concord, MA). The position for steady stirring was determined for each stir plate prior to securing the flask above the stir plate. A Corning magnetic hotplate/stirrer (Model PC420) was used for experiments carried out at 480 and 1100 rpm. OptiCHEM digital hotplate stirrers with stirring control from 50 rpm to 1500 rpm were also used for some experiments. Specially built stirrers equipped with speed controllers (OE Motor Controller or MSRX Speed Controller, PINE Instrument Company) were used to control the stirring rate at 2400 rpm and 4800 rpm. A home-made stirrer equipped with a speed controller (OE Motor Controller) was used to fix the stirring rate at *ca.* 1500 rpm. A Buchler Instruments *Evapo-Mix* vortex shaker operating at *ca.* 3100 rpm was used for the rotary shaking experiment.

PTFE magnetic stir bars (cylindrical; 10 mm x 6 mm) were purchased from Big Science Inc. (Huntersville, NC), 3 mm diameter glass beads (Fischer Scientific, 11-312A) or 0.8 mm diameter YTZ® advanced ceramic materials (also known as Yttria Partially Stabilized Zirconia (Y-PSZ); Tosoh) were used in the abrasion/grinding experiments. The chirality of EDS crystals was determined using a polarimeter (sodium D line) (Autopol II Automatic Polarimeter, Rudolf Research, Fairfield, NJ).

The sources for the amino acids and other chiral additives used in the directed chiral symmetry breaking experiments are listed in Table 3. The solubility of chiral additives is listed in Table 4.

Table 3. List of chiral additives.

Chiral additive	Grade	[CAS]	MW (g/mole)	Formula	Company	Cat. #
D-threonine	Minimum 98% TLC	[632-20-2]	119.12	$C_4H_9NO_3$	Sigma	T8250
L-threonine	N/A	[72-19-5]	119.12	$C_4H_9NO_3$	ICN Biomedicals, Inc.	103053
D-serine	Minimum 98% TLC	[312-84-5]	105.09	$C_3H_7NO_3$	Sigma	S4250
L-serine	ReagentPlus™ ≥ 99%	[56-45-1]	105.09	$C_3H_7NO_3$	Sigma	S4500
D-glutamine	Minimum 98% TLC	[5959-95-5]	146.15	$C_5H_{10}N_2O_3$	Sigma	G9003
L-glutamine	N/A	[56-85-9]	146.15	$C_5H_{10}N_2O_3$	ICN Biomedicals, Inc.	101806
D-alanine	Minimum 98% TLC	[338-69-2]	89.09	$C_3H_7NO_2$	Sigma	A7377
L-alanine	Sigma grade	[56-41-7]	89.09	$C_3H_7NO_2$	Sigma	A7627
D-cysteine	Puriss ≥ 99% (RT)	[921-01-7]	121.16	$C_3H_7NO_2S$	Fluka	30095
L-cysteine	Free base	[52-90-4]	121.16	$C_3H_7NO_2S$	Sigma	C7755
D-leucine	99%	[328-38-1]	131.17	$C_6H_{13}NO_2$	Aldrich	855448
L-leucine	N/A	[61-90-5]	131.17	$C_6H_{13}NO_2$	ICN Biomedicals, Inc.	102158
D-valine	98 +%	[640-68-6]	117.15	$C_5H_{11}NO_2$	Aldrich	855987
L-valine	Reagent grade ≥ 98%	[72-18-4]	117.15	$C_5H_{11}NO_2$	Sigma-Aldrich	V1500
D-proline	99 +%	[344-25-2]	115.13	$C_5H_9NO_2$	Aldrich	858919
L-proline	N/A	[147-85-3]	115.13	$C_5H_9NO_2$	ICN Biomedicals, Inc.	102730
D-isoleucine	Minimum 98% TLC	[319-78-8]	131.18	$C_6H_{13}NO_2$	Sigma	I7634
L-isoleucine	Minimum 98% TLC	[75-32-5]	131.18	$C_6H_{13}NO_2$	Sigma	I2752
D-aspartic acid	99%	[1783-96-9]	133.10	$C_4H_7NO_4$	Aldrich	219096
L-aspartic acid	N/A	[56-84-8]	133.10	$C_4H_7NO_4$	ICN Biomedicals, Inc.	100809
D-glutamic acid	Minimum 99% TLC	[6893-26-1]	147.13	$C_5H_9NO_4$	Sigma	G1001
L-glutamic acid	Minimum 99% TLC	[56-86-0]	147.13	$C_5H_9NO_4$	Sigma-Aldrich	G1251
D-phenylalanine	Minimum 98% TLC	[673-06-3]	165.19	$C_9H_{11}NO_2$	Sigma	P1751
L-phenylalanine	N/A	[63-91-2]	165.19	$C_9H_{11}NO_2$	ICN Biomedicals, Inc.	102323
D-histidine·HCl·H_2O	Minimum 98% TLC	[6341-24-8]	209.63	$C_6H_9N_3O_2$·HCl·H_2O	Sigma	H7625
L-histidine	Free base	[71-00-1]	155.16	$C_6H_9N_3O_2$	ICN Biomedicals, Inc.	101954
D-arginine	Minimum 98% TLC	[175-06-2]	174.2	$C_6H_{14}N_4O_2$	Sigma	A2646
L-arginine·HCl	Sigma grade	[1119-34-2]	210.7	$C_6H_{14}N_4O_2$	Sigma	A5131
D-methionine	Minimum 98% TLC	[348-67-4]	149.21	$C_5H_{11}NO_2S$	Sigma	M9375
L-methionine	N/A	[63-68-3]	149.21	$C_5H_{11}NO_2S$	ICN Biomedicals, Inc.	102291
D-lysine	≥ 98% TLC	[923-27-3]	146.19	$C_6H_{14}N_2O_2$	Sigma	L8021
L-lysine HCl	N/A	[657-27-2]	182.66	$C_6H_{14}N_2O_2$·HCl	ICN Biomedicals, Inc.	102218
D-asparagine·H_2O	Minimum 98% TLC	[5794-24-1]	150.14	$C_4H_8N_2O_3$·H_2O	Sigma	A8131
L-asparagine·H_2O	N/A	[5794-13-8]	150.14	$C_4H_8N_2O_3$·H_2O	ICN Biomedicals, Inc.	100795
D-tyrosine	99%	[556-02-5]	181.19	$C_9H_{11}NO_3$	Aldrich	855456
L-tyrosine	Free base	[60-18-4]	181.19	$C_9H_{11}NO_3$	Fisher Scientific	N/A
D-tryptophan	Minimum 98% TLC	[153-94-6]	204.23	$C_{11}H_{12}N_2O_2$	Sigma	T9753
L-tryptophan	N/A	[73-22-3]	204.23	$C_{11}H_{12}N_2O_2$	ICN Biomedicals, Inc.	103151
D-glucose	A.C.S. reagent	[50-99-7]	180.16	$C_6H_{12}O_6$	Aldrich	25,307-3
L-glucose	Minimum 99%	[921-60-8]	180.16	$C_6H_{12}O_6$	Sigma	G5500
D-tartaric acid	99%	[147-71-7]	150.09	$C_4H_6O_6$	Aldrich	T206
L-tartaric acid	99%	[87-69-4]	150.09	$C_4H_6O_6$	Aldrich	T10-9

Note: L-glutamic acid has to be stored at room temperature in a dessicator; L-glucose has to be stored at 2-8 °C.

Table 4. List of solubilities of chiral additives.

Chiral additive	Solubility in water
D-threonine	Freely soluble in water
L-threonine	Freely soluble in water
D-serine	Soluble in water
L-serine	Soluble in water
D-glutamine	One gram dissolves in 20.8 mL water at 30 °C
L-glutamine	One gram dissolves in 20.8 mL water at 30 °C
D-alanine	166.5 g L^{-1} at 25 °C
L-alanine	166.5 g L^{-1} at 25 °C
D-cysteine	Freely soluble in water.
L-cysteine	Freely soluble in water.
D-leucine	24.26 g L^{-1} at 25 °C
L-leucine	24.26 g L^{-1} at 25 °C
D-valine	88.5 g L^{-1} at 25 °C
L-valine	88.5 g L^{-1} at 25 °C
D-proline	162 grams dissolves in 100 mL water
L-proline	162 grams dissolves in 100 mL water
D-isoleucine	41.2 g L^{-1} at 25 °C
L-isoleucine	41.2 g L^{-1} at 25 °C
D-aspartic acid	One gram dissolves in 222.2 mL water at 20°C
L-aspartic acid	One gram dissolves in 222.2 mL water at 20°C
D-glutamic acid	8.64 g L^{-1} at 25 °C
L-glutamic acid	8.64 g L^{-1} at 25 °C
D-phenylalanine	29.6 g L^{-1} at 25 °C
L-phenylalanine	29.6 g L^{-1} at 25 °C
D-histidine monochloride monohydrate	Fairly soluble in water
L-histidine	41.9 g L^{-1} at 25 °C
D-arginine	15 % (w/w) at 21 °C = 150 g L^{-1}
L-arginine hydrochloride	Soluble in water
D-methionine	33.81 g L^{-1} at 25 °C
L-methionine	33.81 g L^{-1} at 25 °C
D-lysine	Very freely soluble in water
L-lysine monohydrochloride	111.5 g dL^{-1} at 50 °C
D-asparagine monohydrate	3.53% w/w at 28 °C
L-asparagine monohydrate	3.53% w/w at 28 °C
D-tyrosine	0.453 g L^{-1} at 25 °C
L-tyrosine	0.453 g L^{-1} at 25 °C
D-tryptophan	11.4 g L^{-1} at 25 °C
L-tryptophan	11.4 g L^{-1} at 25 °C
D-glucose	One gram dissolves in 1.1 mL water
L-glucose	One gram dissolves in 1.1 mL water
D-tartaric acid	One gram dissolves in 0.75 mL water at room temperature
L-tartaric acid	1390 g L^{-1} water at 20°C

Budavari, S.; O'Neil, M. J.; Smith, A.; Heckelman, P. E. The Merck Index, An Encyclopedia of Chemicals, Drugs, and Biologicals, Centennial Edition. 11th Ed. Merck & Co., Inc. Rahway, N. J. 1989.
Amino Science. www.ajinomoto.co.jp/amino/e_aminoscience/index.html (Accessed on August 16, 2008)

Prior to analyzing the chirality of EDS crystals in solution, a circular plastic grid with small labelled circles was attached to the bottom of the crystallizing dish to separate the analysis area.

Different polarizing microscopes were used to determine the chirality of EDS crystals. A polarizing microscope (Leitz; Laborlux 11 POL S) was used to analyze collected EDS crystals and a polarizing microscope (Nikon SMZ1500; Model C-POL 1003102 polarizer; Model Plan Apo (1X) WD70 analyzer) equipped with a digital camera (Nikon DS-Fi1) was used to analyze EDS crystals directly in the crystallizing dish.

Chemical structures were drawn using ChemDraw. Crystals were drawn using SHAPE (Demo V7.2.1; 2006) and WinXMorph (V1; 2005). The binding orientation of the chiral amino acid on the (001) face was visualized using Mercury (V1.4.2; 2007).

The kinetic graph of the asymmetric amplification study was plotted using Excel and the column graph of directed chiral symmetry breaking was plotted using Origin.

2.1.1. Synthesis of ethylenediammonium sulfate (EDS)

The reaction of ethylenediamine with sulfuric acid is highly exothermic so the reaction must be carried out slowly with continuous ice cooling.

Method 1 - The reaction of ethylenediamine with sulfuric acid was carefully carried out on an ice/salt bath. Ethylenediamine (89 mL; 1.33 moles) was slowly added into a 4 L beaker of ice. Subsequently, concentrated sulfuric acid (98.6%, 71 mL; 1.29 moles) was added dropwise and the resulting mixture was rendered neutral using sulfuric acid or ethylenediamine. Solid EDS (160 g; 2.66 moles) was isolated after lyophilization.

Method 2 – (*N.B.* This method is used for asymmetric amplification and directed chiral symmetry breaking experiments.) Ethylenediamine (99%; 178 mL; 2.66 moles) and ethanol (99%; 750 mL) were added slowly to a 4 L beaker cooled in an ice-bath. Concentrated sulfuric acid (96.8%; 145 mL; 2.64 moles) was added dropwise with continuous stirring. Additional ethanol (2 x 250 mL) was added to the reaction mixture during the synthesis because the reaction mixture became viscous as the product formed and precipitated in the ethanolic solution. Ethylenediammonium sulfate was isolated by vacuum filtration and washed with ethanol (99%; 375 mL) and ether (250 mL). The resulting colorless EDS (320 g, 2.05 mol; 77%) was dried under vacuum overnight and ground into a fine powder with a mortar and pestle prior to use. White EDS powder with a yield of over 80% was obtained.

2.1.2. Preparation of EDS saturated solution (pH 7)

From a 250 mL separatory funnel, a sulfuric acid solution (3 M; 250 mL) was slowly added dropwise (1 to 2 drops/sec) to an ethylenediamine solution (3 M; 250 mL) in a 1 L Erlenmeyer flask (sealed with Parafilm) with continuous stirring under ice cooling. The indication that the solution was saturated was the appearance of precipitate near the end of the addition. Concentrated sulfuric acid (96.8%) or ethylenediamine (99%) was added slowly with constant stirring and under ice cooling to adjust the EDS saturated solution to pH 7. The prepared solution often becomes dark yellow with aging thus causing difficulty in determining the optical rotatory dispersion. In this case, activated charcoal was added to the decanted EDS solution and the solution was vacuum filtered through Celite® filtering agent (Celite® 545; Sigma-Aldrich) on a coarse glass frit. To ensure optimal crystal growth, the saturated solution was shaken vigorously one

day prior to use so that the solution remained at equilibrium. The EDS solution was centrifuged prior to use.

2.2. Chiral crystallization of EDS

Method 1 - From a 100 mL separatory funnel, a sulfuric acid aqueous solution (4.6 M; 50 mL) was slowly added dropwise (1 to 2 drops/sec) to an ethylenediamine aqueous solution (4.6 M; 50 mL) in a 250 mL Erlenmeyer flask (sealed with Parafilm) with continuous stirring under ice cooling. Concentrated sulfuric acid (96.8%) or ethylenediamine (99%) was added slowly with constant stirring and under ice cooling to adjust the resulting unsaturated EDS solution to pH 7. The prepared EDS solution was allowed to cool to room temperature and poured into a crystallizing dish (125 mm x 65 mm). The crystallizing dish was covered with a filter paper and placed in a closed cabinet for crystal growth. This recipe has been optimized for obtaining crystals after *ca.* one week. For example, in one experiment, 7 large single EDS crystals with some crystal clusters were obtained after 7 days.

Method 2 - A similar procedure as Method 1 was performed, except that a more dilute sulfuric acid solution (3 M; 50 mL) was slowly added dropwise (1 to 2 drops/sec) to an ethylenediamine aqueous solution (3 M; 50 mL) in a 250 mL Erlenmeyer flask (sealed with Parafilm) with continuous stirring under ice cooling. The pH adjustment (pH 7) and the crystal growth environment remained the same as described in Section 2.2. This recipe has been optimized for obtaining crystals after *ca.* two weeks.

2.3. Chiral crystallization with exposure to circularly polarized light (CPL)

A blue argon laser beam of 488 nm (0.96 W; 46.6 Amp) was passed through a prism and split into two beams of equal intensity. The light beams were then passed through a quarter-wave plate to become circularly polarized light. The power of the left-CPL beam and the right-CPL beam was 150 – 160 mW. A mirror was used to reflect the light beams downwards onto two crystallizing dishes (50 mm diameter) containing EDS unsaturated solution (0.6 g mL^{-1}). A control experiment in the dark was performed under the same experimental conditions.

2.4. Sealed jar method of crystal growth – (a.k.a. Hope in a jar)

According to the Mason jar/sealed jar method reported by Holden in 1960, large individual crystal can be grown on a thread in supersaturated solution under controlled conditions.[87] An EDS supersaturated solution (pH 7) was prepared by heating a saturated solution with a substantial amount of EDS precipitate at *ca.* 25 °C in a water bath in a partially sealed Erlenmeyer flask. The EDS saturated solution in the water bath was swirled occasionally to maintain a constant concentration for 1 hour. Subsequently the precipitate was allowed to settle to the bottom of the flask in the warm water bath prior to use. The EDS seed crystals were chosen to have a minimum size of 3 mm x 2 mm because smaller crystals often float on the surface of the EDS solution. This EDS seed crystal was attached to a thread (either across the large crystal face or around the slanted edges) using a slip knot (Figure 22)[87] and the extra thread was trimmed. The thread was secured to a cardboard lid (with a diameter slightly larger than the opening of

the jar) using a sewing needle. The length of the thread extending from the cardboard was estimated so that the suspended EDS seed crystal was located *ca.* 2 cm from the bottom of the jar. The top portion of the warmed EDS supersaturated solution was slowly poured into the jar and the attached crystal was immersed into the solution. The opening of the jar was partially covered and the cardboard was secured with Parafilm leaving a partial opening for slow evaporation. The EDS crystal was allowed to grow in an undisturbed environment and the grown crystal was removed if primary nucleation on the bottom of the jar occurred. Using this technique, single EDS crystals with dimensions ranging from (8 mm x 7 mm x 2 mm) to (25 mm x 21 mm x 3 mm) were grown. It is important to note that the density current provides information about the saturation level of the solution. A descending current indicates crystal dissolution which means that the solution is unsaturated. An ascending current indicates crystal growth which means that the solution is supersaturated.[87]

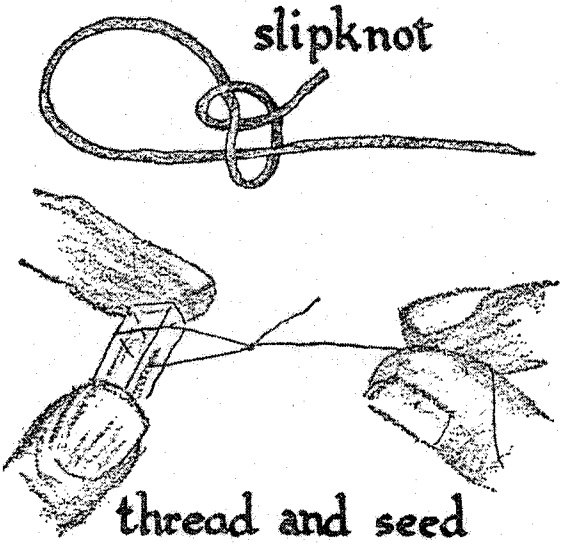

Figure 22. Schematic representation of a slip knot.[87]

2.5. Stirred crystallization of EDS

In a 5 mL glass vial (20 mm diameter), 1 mL of the middle portion of freshly centrifuged EDS saturated solution (pH 7) and 50 μL of distilled water were stirred at *ca.* 1000 rpm with a Teflon magnetic stir bar (10 mm x 6 mm) using an OptiCHEM digital stirrer. The glass vials were covered with a layer of Kimwipe to avoid contamination. Crystalline seeds were observed on the next day and the vials were sealed with Parafilm when the stirrer was stopped.

2.6. Closed system set up for the abrasion/grinding technique

A sample of EDS powder with or without chiral additive was stirred in the presence of grinding media in a closed Erlenmeyer flask or glass vial.

2.6.1. Abrasion/grinding with glass beads

Abrasion/grinding with glass beads: *ca.* 0.5 g of EDS powder, 1.2 mL of saturated EDS solution, *ca.* 1.0 g of glass beads (3 mm diameter; Fischer Scientific), and a magnetic stir bar (10 mm x 6 mm) were added to a 5 mL round bottom flask which was closed with a glass stopper. The abrasion/grinding mixtures were stirred at *ca.* 480 rpm and *ca.* 1100 using Corning magnetic stirrers until homochirality was reached.

2.6.2. Abrasion/grinding with ceramic beads

Abrasion/grinding with ceramic beads: *ca.* 0.25 g of EDS powder, 1.0 mL of saturated EDS solution, *ca.* 3.0 g of YTZ® Zirconia grinding media (0.8 mm diameter; Tosoh Corporation), and a magnetic stir bar (10 mm x 6 mm) were added to a 5 mL round bottom flask which was closed with a glass stopper. The abrasion/grinding

mixtures were stirred at *ca.* 2400 rpm and 4800 rpm using a home-made stirrer equipped with OE speed controller or MSRX speed controller. Some experiments were performed at *ca.* 3100 rpm using an *Evapo-Mix* vortex shaker.

2.6.2.1. Determination of errors in kinetic study

Error bars in the plot of CEE versus time of stirring (Figure 25) were calculated for each point by pooling 150 crystals into three groups of 50. The number of *dextrorotatory* and *levorotatory* crystals in each pool was used to obtain three values of the crystal enantiomeric excess (CEE) at each time. The average value at each time was used as the data point and the standard deviation of each set was used as the magnitude of the error bars above and below the data point. It was not possible to calculate error bars for the kinetic study performed at 480 rpm using 3 mm diameter glass beads, in our initial experiments, the data was grouped into only one pool.

2.6.2.2. Estimation of the sampling pool size for chirality analysis

A scatter plot was plotted with %CEE versus the number of crystals in the sampling pool for 680 crystals grown from racemic seeds (*i.e.* prior to the abrasion/grinding experiment). This plot is meant to illustrate that a sufficiently large number of crystals should be analyzed to account for the error associated with counting random events.

2.6.3. Abrasion/grinding with ceramic beads in the presence of chiral additive

Abrasion/grinding with ceramic beads in the presence of amino acids: *ca.* 0.25 g of EDS powder, chiral amino acid (an amount between the half and its maximum solubility in water), 1.0 mL of saturated EDS solution, *ca.* 3.0 g of YTZ® Zirconia

grinding media (0.8 mm diameter), and a magnetic stir bar (10 mm x 6 mm) were added to a 5 mL round bottom flask and sealed with a glass stopper. For glucose and tartaric acid, an amount between the half and its maximum solubility in water was added to the abrasion/grinding system. The abrasion/grinding experiments were carried out using a home-made stirrer equipped with an OE speed controller at *ca.* 1500 rpm or using an *Evapo-Mix* vortex shaker operating at *ca.* 3100 rpm under water cooling.

The average concentration of chiral additives is listed in Table 5. Five different amounts of EDS powder (0.25 g, 0.18 g, 0.125 g, 0.08 g, and 0.05 g) were used in the 242 experiments. In some cases, a smaller amount of EDS powder was added in the closed system setup to increase the ratio of chiral additive to EDS. It is believed that increasing the ratio of chiral additive to EDS may increase the probability of enantioselective adsorption on the EDS crystal surface. Moreover, a slight increase in temperature was observed during the abrasion/grinding process which is believed to be caused by friction due to the constant stirring or shaking in the presence of grinding media. Therefore, a larger amount of EDS powder (0.25 g and 0.18 g) was chosen when using the high speed vortex shaker to ensure that the solid was not completely dissolved due to increased temperature. The sample mixture was stirred or shaken at a controlled rate in the presence of grinding media. Seeding of crystallites in freshly prepared saturated solution was carried out. In each experiment, seeds were sampled after *ca.* 4 days of abrasion/grinding and were allowed to grow to a larger size in EDS saturated solution for subsequent analysis.

Table 5. Average concentration of chiral additives used in abrasion/grinding experiments.

Chiral additive	Average concentration (M)
D-threonine	3.40E-01
L-threonine	3.20E-01
D-serine	3.40E-01
L-serine	2.73E-01
D-glutamine	2.50E-01
L-glutamine	1.71E-01
D-alanine	8.11E-01
L-alanine	8.04E-01
D-cysteine	8.27E-02
L-cysteine	7.18E-02
D-leucine	1.40E-01
L-leucine	1.12E-01
D-valine	4.70E-01
L-valine	4.26E-01
D-proline	4.42E-01
L-proline	7.49E-01
D-isoleucine	1.86E-01
L-isoleucine	2.24E-01
D-aspartic acid	3.03E-02
L-aspartic acid	2.88E-02
D-glutamic acid	4.13E-02
L-glutamic acid	3.55E-02
D-phenylalanine	1.24E-01
L-phenylalanine	1.19E-01
D-histidine monochloride monohydrate	1.39E-01
L-histidine	1.85E-01
D-arginine	3.14E-01
L-arginine hydrochloride	3.19E-01
D-methionine	1.49E-01
L-methionine	1.38E-01
D-lysine	1.75E-01
L-lysine monohydrochloride	1.89E-01
D-asparagine monohydrate	1.21E-01
L-asparagine monohydrate	1.21E-01
D-tyrosine	2.76E-03
L-tyrosine	3.25E-03
D-tryptophan	3.10E-02
L-tryptophan	4.06E-02
D-glucose	1.22
L-glucose	3.62E-01
D-tartaric acid	9.36E-01
L-tartaric acid	1

Ten control abrasion/grinding experiments were performed with EDS in the absence of additive using an *Evapo-Mix* vortex shaker. Based on our experiments, abrasion/grinding with either stirring or shaking both give the same results with respect to chiral symmetry breaking and chiral amplification. In this work, both techniques were used in order to speed up the data collection process.

2.7. Chiral symmetry breaking using circularly polarized light

Abrasion/grinding experiments without chiral additives with exposure to circularly polarized light were prepared as described in section 2.6.2. and were stirred using an OptiCHEM stirrer at 1500 rpm. A green laser beam (YAG: yttrium aluminium garnet) of 532 nm with an area of 1.65 cm^2 passed through a prism and split into two light beams of 30 mW. Then the light beams passed through a quarter-wave plate to become CPL. The power of the CPL of the right side and the left side became 18.7 mW and 7.5 mW, respectively. The CPL was positioned at the abrasion/grinding mixture and a black cardboard was placed between the experiments to avoid contamination with opposite CPL.

2.8. Crystal seeding technique

Ethylenediammonium sulfate crystallites (*ca.* 7 μL) were sampled from the abrasion/grinding mixture at various times using an automatic pipette and transferred to the bottom of a 125 mL Erlenmeyer flask containing about 100 mL of freshly centrifuged EDS saturated solution (pH 7). The Erlenmeyer flask was quickly sealed with Parafilm and swirled slightly to disperse the crystallites. The presence of the seeds was monitored for *ca.* 15 minutes prior to pouring the solution into a crystallizing dish (100 mm x

50 mm). To determine the final chirality of crystals from stirred crystallization and abrasion/grinding experiments, the crystalline seeds were allowed to grow for one day to avoid dissolution during subsequent seeding. The crystallizing dish was partially covered with filter paper and allowed to sit undisturbed for crystal growth. After 1 to 2 days individual crystals were collected (*ca.* 150 crystals with average dimensions of *ca.* 1.6 mm x 1.6 mm x 0.3 mm) and analyzed using a polarized light microscope. Although all attempts were made to minimize the possibility of primary nucleation (yielding racemic crystals) during the seeding experiments, one cannot exclude this possibility. Primary nucleation would influence the CEE data more significantly as one approaches homochirality.

2.9. Determination of EDS crystal chirality

Crystals were either analyzed individually after removal from the saturated solution or they were directly analyzed in the crystallizing dish using a polarizing microscope. Direct analysis of EDS crystals in saturated solution was performed using a circular plastic grid of the same diameter as the crystallizing dish. This plastic grid with small circles divides the bottom of the crystallizing dish into labelled areas and the chirality of all EDS crystals in each labelled area was examined using a polarizing light microscope (Nikon, model: SMZ1500, integrated with a Nikon DS-Fi1 digital camera). Since this plastic grid also behaves as a polarizing film, the grid must be rotated to allow sufficient light to pass through the crystals. The analyzer was rotated clockwise to determine the optical rotatory dispersion of individual crystals.

The optical rotatory dispersion of the crystals was examined as follows: a color change from clear to blue to amber indicates *dextrorotatory* EDS crystals and a color

change from amber to blue to clear indicates *levorotatory* EDS crystals. The crystal enantiomeric excess (CEE) for each sample was calculated according to equation 4.

Over 200 experiments were performed and the number of EDS crystals examined in each experiment varied from 20 to 500 crystals. The selection criteria for including data in our final results required that: (*i*) at least 20 crystals were counted in each experiment, and (*ii*) a CEE of greater than 90% was obtained. All 19 pairs of chiral amino acids were examined and multiple experiments for each pair of amino acid were carried out ($n \geq 3$). The results reported in Figure 27 incorporate abrasion/grinding experiments using both high speed stirring and shaking.

2.10. Molecular modeling

Some preliminary modeling of the adsorption of amino acids on the (0 0 1) face of EDS crystal was done using the CHARMM software.[88] The model system is represented by a 36 Å x 36 Å x 72 Å simulation cell with periodic boundary conditions. Each cell contains two components: (*i*) a crystal slab of 6 x 6 x 2 copies of the unit cell (which contains four diethylammonium-sulfate pairs, and measures 6 Å x 6 Å x 18 Å), and (*ii*) one amino acid molecule in its zwitterionic form. The amino acid is positioned randomly in the vacuum layer between the 18 Å thick crystal slab and its periodic image 72 Å above.

The molecular interactions are calculated with the standard PARAM27 force field[89] for the amino acids and for ethylenediammonium, and model "std 1" from Cannon, Pettitt, and McCammon[89] for the sulfate ion.

The binding energy (E_{bind}) is calculated using the following formula:

$E_{bind} = E(aa + xtl) - E(aa) - E(xtl)$

where E(aa) is the potential energy of the 36 Å x 36 Å x 72 Å simulation cell containing only the amino acid, E(xtl) is the potential energy of the simulation cell containing only the crystal, and E(aa + xtl) is the potential energy of the simulation cell containing both the amino acid and the crystal.

The general procedure to sample E(aa + xtl) is the following:

(*i*) The amino acid molecule was placed at 8 Å above the crystal surface, at a random X-Y position and in a random orientation.

(*ii*) The overall structure of the aa + xtl system was optimized with 1000 steps of the adopted basis Newton-Raphson (ABNR) energy minimization method.[90] Each atom of the crystal is kept rigidly at its crystallographic position, except for the top layer (the top ED-S pair of each unit cell). This allows the surface of the crystal to accommodate a specific interaction with the amino acid.

(*iii*) The amino acid molecule adsorbs to the surface in a pose that depends on its initial orientation. To sample the various possible poses, the procedure was repeated 100 time or 1000 times for each amino acid (and each isomer).

(*iv*) The optimized poses are ranked according to their E(aa + xtl) values (the lowest being the most stable).

2.11. Identification of crystal faces

Individual EDS crystals were grown to a larger size in crystallizing dishes or by using the sealed jar method to facilitate the indexing of crystal faces.[87] Most of the large crystal faces were indexed using a contact goniometer and the smaller and hidden faces were indexed using powder x-ray diffraction. X-ray powder diffraction (XRPD) patterns were measured using a Scintag XDS-2000 Diffractometer equipped with a Si(Li) Peltier-cooled solid state detector, CuKα source at a generator power of 45 kV and 40 mA, divergent beam (2 mm and 4 mm) and receiving beam slits (0.5 mm and 0.2 mm). The scan range was set from 20-80° 2θ with a step size of 0.02° and a count time of 2 sec. The sample was measured using a quartz zero background insert disk.

Chapter 3. Results and Discussion

> Winnie-the-Pooh read the two notices very carefully, first from left to right, and afterwards, in case he had missed some of it, from right to left.
>
> *Winnie-the-Pooh*
> A.A. Milne

3.1. Complete asymmetric amplification of EDS

Previous studies of chiral crystallization of EDS showed that the slow crystallization of ethylenediammonium sulfate from an aqueous solution gives a statistically equal number of *dextrorotatory* and *levorotatory*, as expected.[91] Both enantiomers have an equal probability to be crystallized from primary nucleation. Among the 100 individual crystals collected, 47 crystals were *dextrorotatory* and 53 crystals were *levorotatory*. The average optical rotation (15° mm^{-1} ± 2) agrees with the literature value.[86] A study of chiral crystallization of EDS was performed in the presence of circularly polarized light (CPL) at 488 nm (Figure 23). Due to the small number of crystals obtained in the crystallizing dishes the experimental results are not conclusive.

Figure 23. Chiral crystallization of EDS with exposure to circularly polarized light.

The mirror symmetry breaking and chiral amplification of EDS were carried out using stirred crystallization. Among the two experiments, one experiment led to the formation of *dextrorotatory* EDS crystals with 94.9% CEE and one experiment led to the formation of *levorotatory* EDS crystals with 97.9% CEE. It is important to note that most results obtained from our initial EDS starting material led to homochiral *levorotatory* EDS crystal under abrasion/grinding. This first attempt of stirred crystallization without the presence of solid EDS starting material shows an important piece of information to support our explanation of slight enantiomeric excess in the EDS starting material. If the results are reproducible, it indicates that both enantiomorphous crystals have an equal chance to form during primary nucleation as expected and secondary nucleation will be induced under constant stirring. More experimental data is required to confirm the stochastic formation of chiral EDS crystals in stirred crystallizations.

The asymmetric amplification of EDS was studied using an abrasion/grinding technique first reported by Viedma.[46] Apart from the experiments on sodium chlorate and sodium bromate reported by Viedma, to our knowledge this is the only other example

to date of asymmetric amplification by thermodynamic/kinetic feedback near equilibrium.[92] Complete asymmetric amplification of EDS was achieved at different stirring rates using either 3 mm glass beads or 0.8 mm ceramic beads as grinding media and a high CEE of 94 to 100% was obtained.[93] A schematic representation of asymmetric amplification using an abrasion/grinding technique is shown in Figure 24.

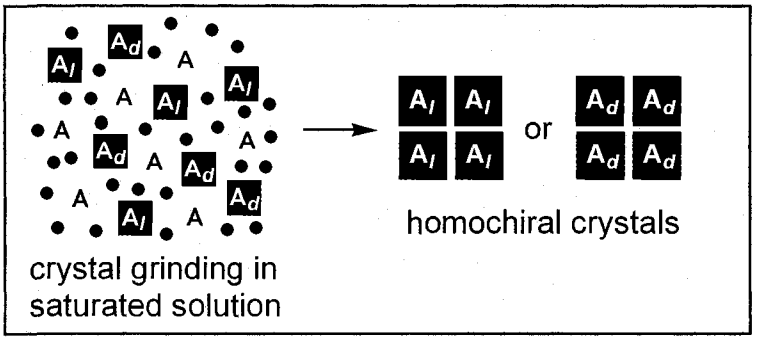

Figure 24. Schematic representation of asymmetric amplification using the abrasion/grinding technique. Black dots represent grinding media, the letter 'A' represents achiral molecules, black A_d squares represent *dextrorotatory* crystals, and black A_l squares represent *levorotatory* crystals.

The duration of stirring required to reach chiral purity under different experimental conditions shows that homochirality is attained in less time at higher stirring rates. The time required to obtain complete asymmetric amplification using 3 mm glass beads as grinding media was *ca.* 20 days and *ca.* 7 days with stirring rates of 480 rpm and 1100 rpm, respectively. Clearly, there is a significant decrease in time to achieve complete asymmetric amplification as the stirring rate is increased. It is interesting to note that the rate of asymmetric amplification of EDS is much slower than that of sodium chlorate where chiral purity is achieved after *ca.* 1 day at 600 rpm with 3 mm glass beads.[46] In order to increase the rate of asymmetric amplification further, smaller diameter grinding media were used. With stirring rates of 2400 rpm and 4800 rpm using 0.8 mm ceramic beads as grinding media, homochirality was achieved after *ca.* 3 days and *ca.* 1.5 days,

respectively. When the kinetics of the process were monitored, an asymptotic trend was observed during the nonlinear autocatalytic process (Figure 25).[93] Complete asymmetric amplification was also achieved after *ca.* 6 days using a vortex shaker operating at *ca.* 40 Hz (2400 rpm) with 0.8 mm diameter ceramic beads as grinding media. To briefly summarize these results, the time required to achieve homochirality depends on both the size of the grinding media and the stirring rate.

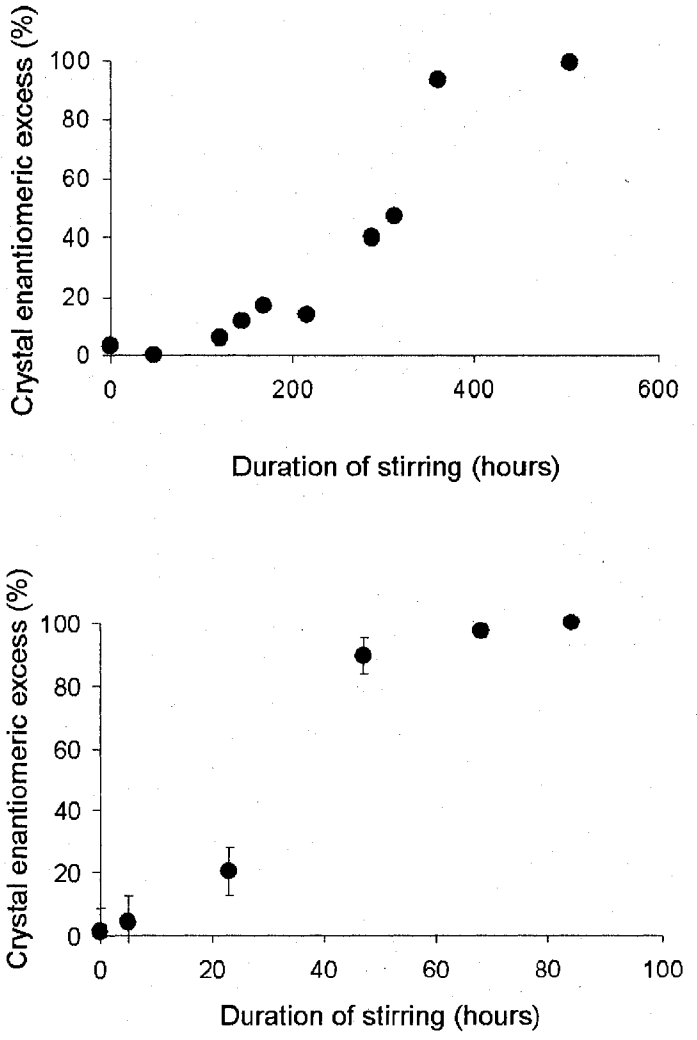

Figure 25. Complete asymmetric amplification of EDS by abrasion/grinding technique.[93] Evolution of CEE with time using 3 mm glass beads as grinding media with a stirring rate of 480 rpm (top); evolution of CEE with time using 0.8 mm ceramic beads as grinding media with a stirring rate of 2400 rpm (bottom).

The results for eight separate experiments demonstrate a handedness preference towards *levorotatory* crystals. This is due to the fact that the chirality of the starting material prepared in our lab has a 4.5% CEE of *levorotatory* crystals as determined by the seeded growth of 2177 crystals. We were unable to synthesize a true racemic mixture of EDS starting from ethylenediamine and sulfuric acid. This may be due to the presence of trace chiral impurities (cryptochiral environment) in our laboratory as was also described for the directed asymmetric amplification observed by Viedma for sodium chlorate and sodium bromate.[51] We propose that a cryptochiral environment during the synthesis of ethylenediammonium sulfate causes an initial chiral imbalance in our starting material. Asymmetric amplification towards both *dextrorotatory* and *levorotatory* crystals was observed when an equal mixture of ground *dextrorotatory* and *levorotatory* EDS crystals was used as the starting material for the grinding/abrasion experiment. Furthermore, when the initial mixture was purposely biased with an excess of one chiral form of the crystals (20% CEE), the asymmetric amplification of the EDS crystals was directed towards the original bias as expected. The mechanism of asymmetric amplification of EDS is thought to involve the same steps as described by Viedma for the asymmetric amplification of sodium chlorate.[94] First, the EDS crystals in saturated solution experience continuous dissolution/recrystallization under abrasion/grinding in the closed system where small fragments are broken off from the initial crystals during the grinding process. According to the Gibbs-Thompson equation, small crystallites have a higher solubility than larger ones and therefore dissolve more readily into achiral molecules which can subsequently add to existing crystals. This recycling process is critical since any enantiomeric imbalance will be amplified at the expense of the handedness in

minority in a nonlinear manner *via* Ostwald ripening.[92] Concisely, the direction of symmetry breaking of a racemic system depends on chance during the abrasion/grinding process and the associated recycling process amplifies this initial broken symmetry towards homochirality.

An important aspect in asymmetric amplification studies is the relationship between the distribution of %CEE and the amount of EDS crystals analyzed in each experiment. Statistically, the %CEE of an asymmetric amplification experiment is closer to its true value when a large enough amount of EDS crystal sample is analyzed. A scatter plot was plotted with %CEE versus the number of crystals in the sampling pool for 680 crystals grown from racemic seeds (*i.e.* prior to the abrasion/grinding experiment) (Figure 26). This plot shows that the variation of %CEE increases as the sampling pool size decreases and clearly illustrate that a sufficiently large number of crystals should be analyzed to account for the error associated with counting random events.

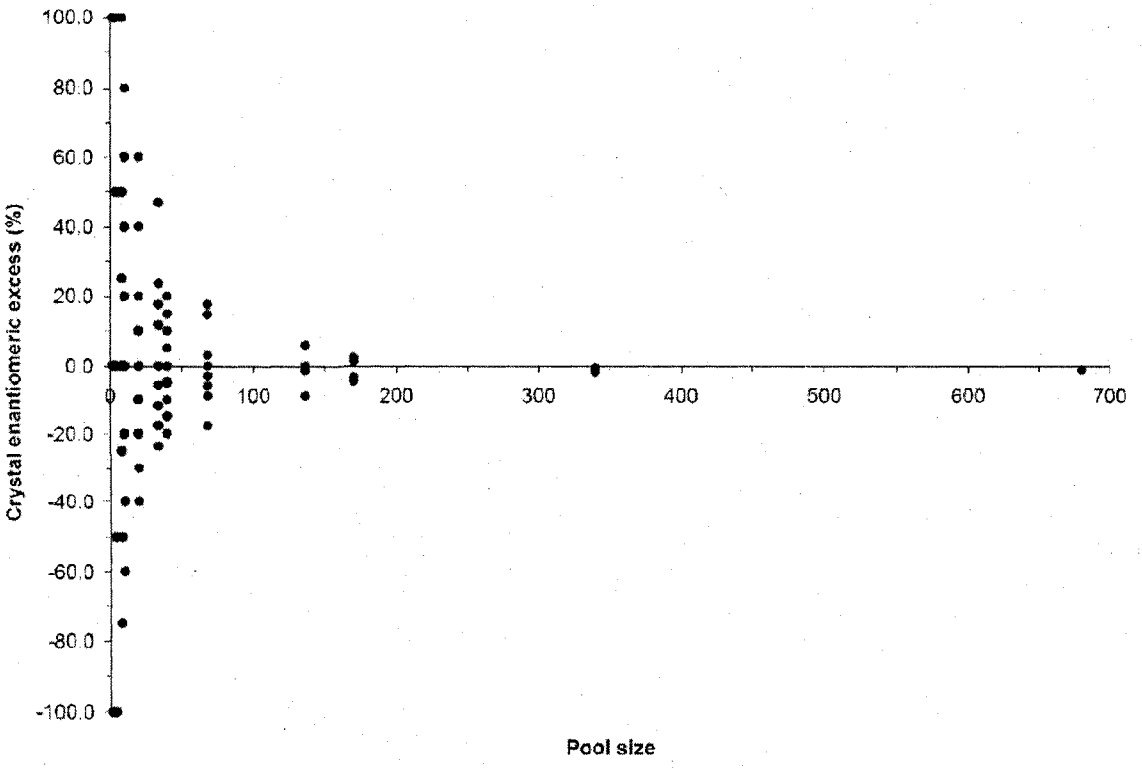

Figure 26. Scatter plot of %CEE versus sample pool size.[93] Each column shows all the calculated %CEE values in each pool. Each column represents the same total number of crystals where the number of points in each column is equal to 680/pool size (*N.B.* in many cases there are overlapping points).

Our experimental results showed that the resulting chirality from a complete asymmetric amplification of EDS can be influenced by the presence of hidden impurities. What if we purposely incorporate a chiral additive in the abrasion/grinding closed system of EDS?

3.2. Directed chiral symmetry breaking of EDS

The investigation of the influence of chiral amino acid additives on the chiral symmetry breaking and amplification process of EDS was carried out using an abrasion/grinding technique as described previously. The direction of the chiral symmetry breaking of EDS was examined using a simple experimental approach where chiral amino acids were directly incorporated into an abrasion/grinding chiral

amplification system. A summary of the directed chiral symmetry breaking results is shown in Figure 27.

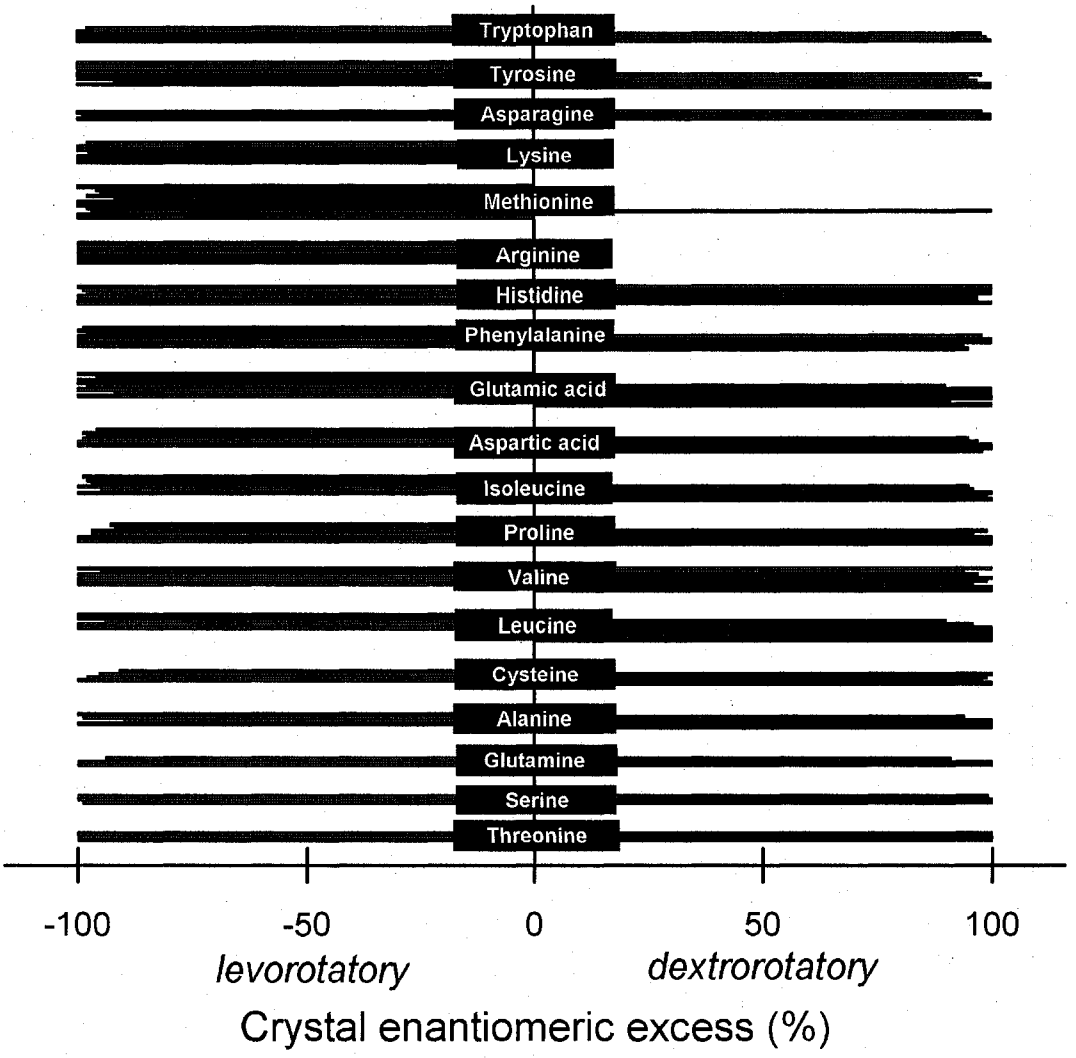

Figure 27. Directed chiral symmetry breaking of EDS with chiral amino acids. Each column represents one experiment of directed chiral symmetry breaking of EDS in the presence of a chiral amino acid. Blue or red columns represent experiments with the addition of D-amino acids or L-amino acids in the chiral amplification system, respectively.

Varying degrees of directed chiral symmetry breaking were observed and the amino acids can be separated into three main groups: (*i*) for threonine, serine, glutamine, alanine, cysteine, leucine, valine, proline, isoleucine, aspartic acid, glutamic acid, phenylalanine,

and histidine, the addition of D-amino acids mostly directed the chiral symmetry breaking towards homochiral *dextrorotatory* EDS crystals whereas the addition of L-amino acids mostly directed the process towards homochiral *levorotatory* EDS crystals; (*ii*) for arginine, methionine, and lysine, the presence of D- or L-amino acids showed no directing effect and therefore led to homochiral *levorotatory* EDS crystals as observed in our study of complete asymmetric amplification[93]; on the other hand, (*iii*) for asparagine, tyrosine, and tryptophan, the addition of D-amino acids directed the chiral symmetry breaking process towards homochiral *levorotatory* EDS crystals while the addition of L-amino acids directed the chiral symmetry breaking towards homochiral *dextrorotatory* EDS crystals. These trends show that the direction of the symmetry breaking of EDS is strongly dependent on which chiral amino acid is present and its chirality.

From our previous work, we found that the 'racemic' starting material prepared in our laboratory has a slight excess of the *levorotatory* enantiomer (*ca.* 4%). Therefore, when there is no effect of the chiral amino acid on the symmetry breaking and chiral amplification of EDS, or if the opposing effect is not sufficiently strong, the chirality of the EDS is expected to be amplified to homochiral *levorotatory* crystals. However, as clearly observed from the results in Figure 27, this initial bias (*i.e.* broken symmetry) for *levorotatory* crystals can often be reversed in the presence of the appropriate amino acid. It is believed that the chirality of the amino acids and their unique side chains play an important role in the molecular adsorption on the surface of EDS crystals.

The classic sketch of, "a left and a right hand and two enantiomorphous tetrahedra" by Hans Erni in Prelog's Nobel lecture illustrates the importance of the nonlinear three point contact in chiral recognition (Figure 28).[95, 96] It is believed that the

direction and mechanism of the symmetry breaking process reported here also relies on the nonlinear three point contact principle. For example, this diastereomeric interaction can be demonstrated by the carboxylic acid group, the amino group and the side chain of an amino acid interacting with a chiral crystal surface (Figure 29).[97]

Figure 28. A classic sketch of "a left and a right hand and two enantiomorphous tetrahedra" by Hans Erni.

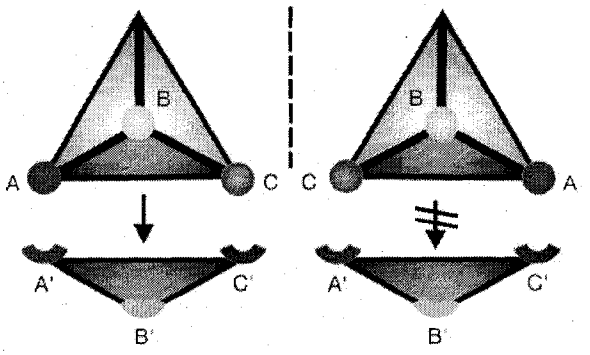

Figure 29. Illustration of the enantioselective adsorption according to the three point contact principle. A molecule with sites (A, B, C) interacts with its respective recognition sites (A', B' and C') (left); the mirror image of the same molecule cannot interact with the same recognition sites (right).

Similarly, the enantioselective adsorption of a chiral molecule on a chiral EDS crystal surface can be illustrated as shown in Figure 30. To study these types of interactions, it is important to understand the molecular presentation at the relevant crystalline faces of EDS.

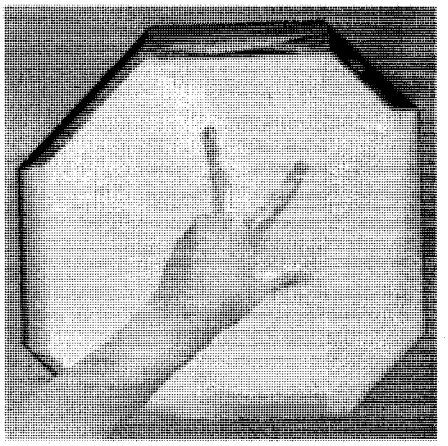

Figure 30. Illustration of the enantioselective adsorption of a chiral molecule on an EDS crystal.

In our work, the D- or L-amino acid is expected to have a different strength of interaction for the same EDS crystal surface which subsequently leads to chiral selection. The adsorption of chiral amino acids on selective chiral faces of EDS crystals may hinder crystal growth or may trigger crystal dissolution at the adsorption site[56] so that the opposite crystal chirality is amplified during the Ostwald ripening and recycling process. Other chiral molecules have also been investigated. Although the addition of D-tartaric acid and L-tartaric acid showed no observable effect, the presence of D-glucose or L-(-)-glucose directed the chiral symmetry breaking of EDS towards homochiral *dextrorotatory* or *levorotatory* crystals, respectively.

If our concept of enantioselective adsorption on chiral EDS crystal surfaces is correct, the following possibilities are proposed to explain the direction of chiral symmetry breaking of EDS. In the case of the incorporation of one of the thirteen amino acids (Figure 27), D-amino acids preferentially adsorb on *levorotatory* EDS crystals so that the *dextrorotatory* EDS crystals are amplified to homochirality during the recycling process; whereas L-amino acids preferentially adsorb on *dextrorotatory* EDS crystals so

that the *levorotatory* EDS crystals are amplified to homochirality during the recycling process. The opposite enantioselective adsorption is expected for the case of asparagine, tyrosine and tryptophan where the D-amino acids preferentially adsorb on *dextrorotatory* EDS crystals whereas L-amino acids preferentially adsorb on *levorotatory* EDS crystals, so that the EDS crystals with lower molecular adsorption will be amplified. This directed chiral symmetry breaking of EDS in the presence of chiral additive is illustrated in a simplified schematic representation as shown in Figure 31. The enantioselective adsorption of chiral additives on chiral EDS crystals requires further investigations to support our experimental results.

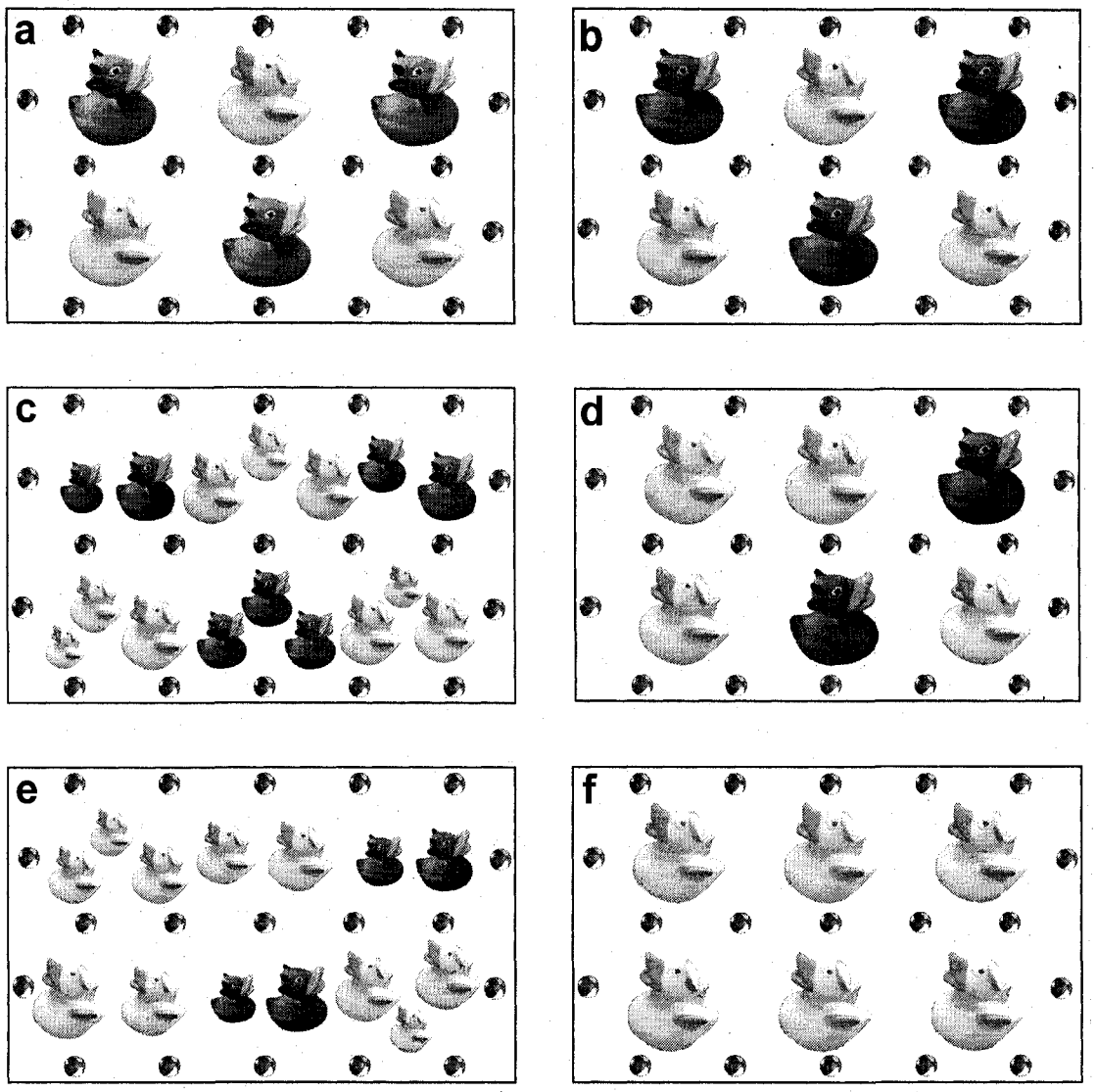

Figure 31. A proposed model of the directed chiral symmetry breaking process. (a) A racemic mixture of 50% *dextrorotatory* (red devil ducks) and 50% *levorotatory* crystals (white angel ducks) in saturated solution in the presence of grinding media (beach balls). (b) The preferential adsorption of an L-amino acid on *dextrorotatory* crystals is illustrated by the darkening of the red devil ducks. The amino acid adsorption is believed to slow down the growth or trigger the dissolution of the red devil ducks. (c) Under constant stirring, the chiral crystals are broken down into smaller crystals of the same chirality. These smaller crystals dissolve more easily into achiral molecules. (d) These resulting achiral molecules feed growing crystals in the system independently of their chirality during Ostwald ripening. The dominating angel ducks grow at the expense of the devil ducks. (e) The recycling process amplifies the number of angel ducks. (f) Eventually only white angel ducks remain at the end (homochirality).

The influence of another kind of chiral initiator, circularly polarized light at 532 nm, was examined on the chiral symmetry breaking of EDS using the abrasion/grinding technique (Figure 32). Our first two results showed homochiral *levorotatory* EDS crystals for both the right-CPL and left-CPL experiments. If there is an effect of CPL on the chiral symmetry breaking process perhaps this effect is not strong enough to overcome the initial bias of excess *levorotatory* EDS in our starting material. More experimental data is required to further interpret the possible effects of CPL on our chiral symmetry breaking system.

Figure 32. Chiral symmetry breaking and asymmetric amplification of EDS using the abrasion/grinding technique with exposure to circularly polarized light.

The preliminary modeling study of binding energy differences of chiral amino acids on the (001) face of EDS crystals was performed in vacuum using the CHARMM software. The binding energies did not show any particular trend that correlates with our experimental results (Figure 33). It is believed to be due to the absence of solvent in the modeling environment. The lack of interactions between the solvent and the charged

molecules (*i.e.* a screening effect) is absent and therefore does not completely represent the experimental conditions.

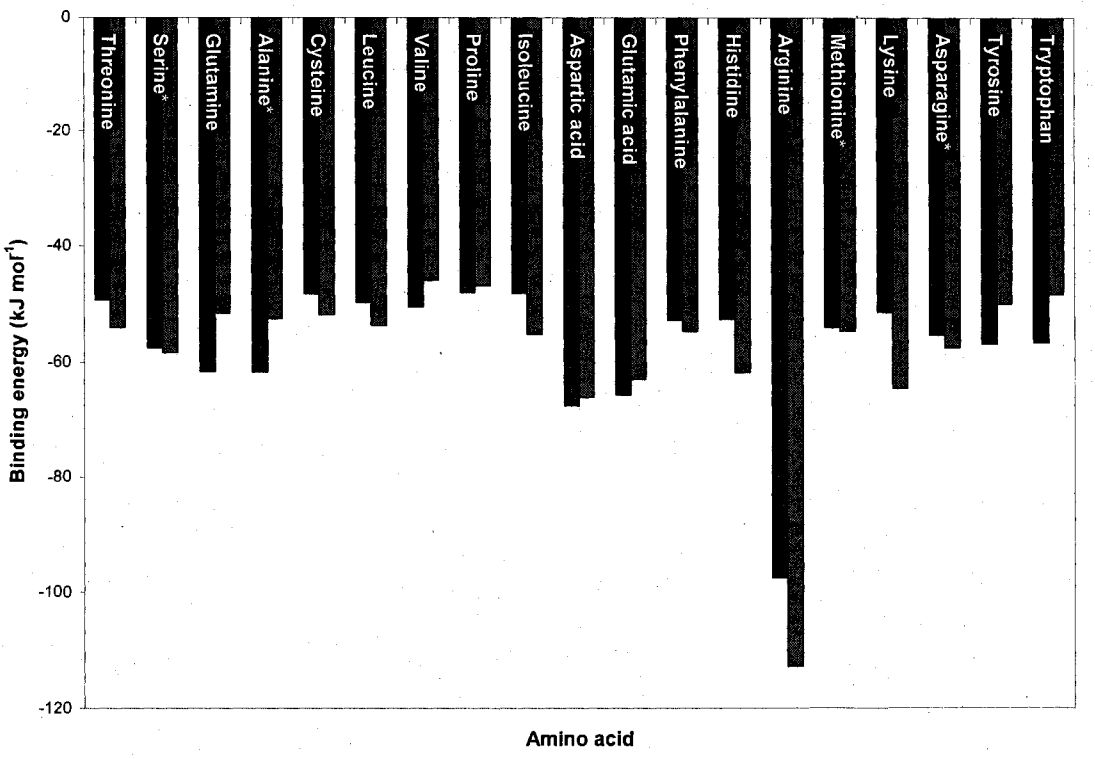

Figure 33. Binding energy of chiral amino acid on the (001) face of an EDS crystal using the CHARMM software. Amino acids with an asterisk (*) were analyzed with 500 trials and the other amino acids were analyzed with 50 trials, for each enantiomer.

In order to further understand the preferential adsorption of chiral molecules on different faces of EDS crystals, the crystal morphology of EDS has to be investigated in greater detail. Using single crystal x-ray diffraction, the unit cell dimensions were confirmed to agree with those reported in the literature.[85] Also, this technique was used to identify the top face of EDS crystals as shown in Figure 34 as the (001) face.

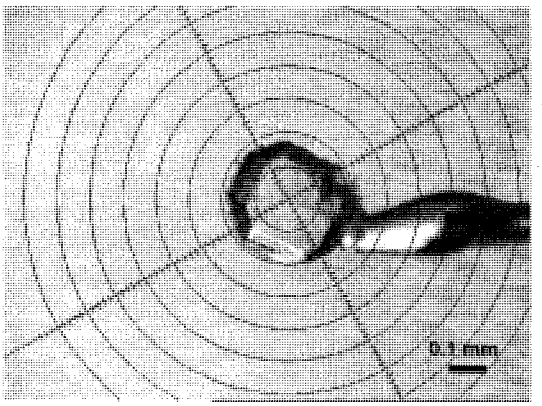

Figure 34. The (001) face of an EDS crystal mounted in a diffractometer goniometer.

This experiment required very small single crystals that are hard to see with the naked eye. But information can also be obtained from large crystals such as the one shown in Figure 35.

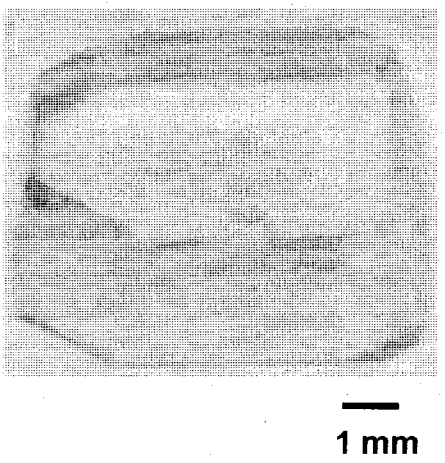

Figure 35. Large single EDS crystal obtained from chiral crystallization.

Large individual EDS crystal can be obtained using the crystallization method similar to the procedure mentioned in section 2.2 (*N.B.* larger crystallizing dishes and lower initial concentrations were used to obtain large individual crystals) or using the sealed jar method as shown in Figure 36.

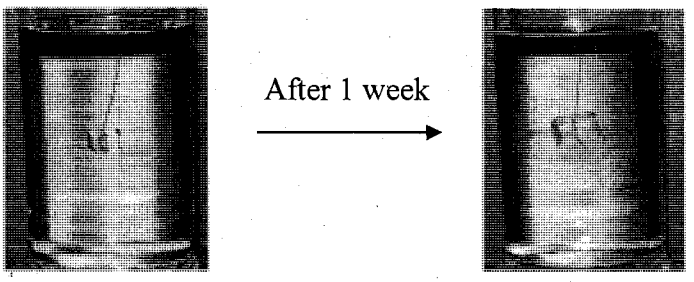

Figure 36. Growth of an EDS crystal using the sealed jar method.

By inspecting many large crystals, most of the major crystalline faces can be identified. With the EDS crystal shown in Figure 35, a total of 28 faces were identified and a schematic representation was drawn using ChemDraw (Figure 37).

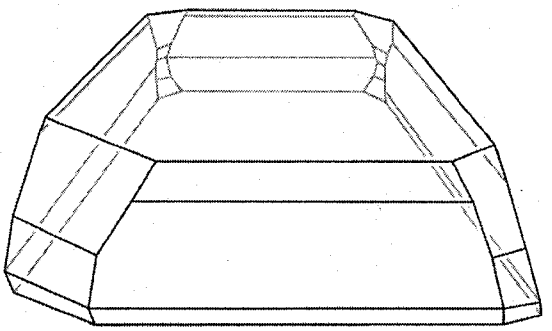

Figure 37. Schematic representation of the EDS crystal shown in Figure 35.

Wherever possible, the angles between two crystalline faces were measured using a contact goniometer. Using trigonometry most of the large crystalline faces were identified according to Figure 38.

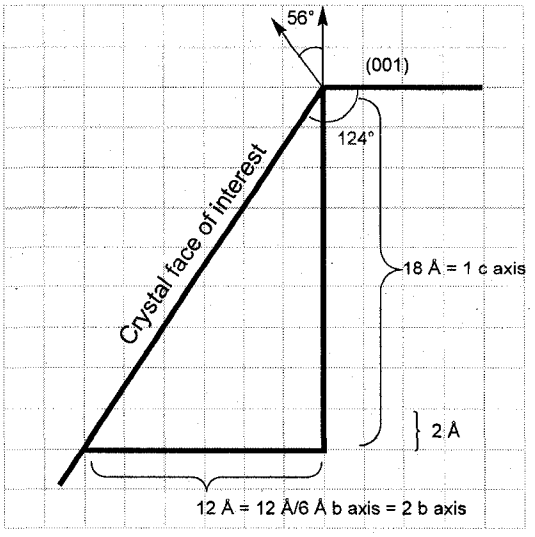

Figure 38. Trigonometric calculation of a Miller index.

intercept	∞ a,	2b,	1c	
1/intercept	0	1/2	1/1	
		↓		X 2 to obtain an integer value
	h	*k*	*l*	
Miller index	(0	1	2)	

The angle between the (001) face and the crystal face of interest was measured using a contact goniometer where this specific example shows an angle of 124°. A horizontal line is drawn which represents the reference (001) face of the EDS crystal (Figure 35 and Figure 37) and the crystal face of interest is drawn as shown in figure Figure 38. The reported dimensions of the EDS unit cell are 5.9993 Å for the a- and b-axes and 18.047 Å for the c-axis.[85] For calculation purposes, the dimensions of the unit cell are estimated to be 6 Å and 18 Å.

Each square on the graph represents 2 Å and the length of the b- and c-axes on the graph is drawn proportionally to the lengths of the unit cell. A vertical line is drawn from the intersection point (between the (001) face and the unknown face) according to its length (in unit cell dimensions) to represent the c-axis. The end of this c-axis is extended horizontally until intercepting the crystal face of interest to represent the b-axis. The a-axis is considered to be infinity because it does not intercept with the crystal face of interest. The reciprocal of the ratios of the length of the b- and c-axes obtained from the graph paper was carried out to obtain the Miller indices (*h*, *k*, *l*). Since fractional values were obtained, the values have to be doubled to obtain the smallest integer values. So, the crystal face of interest is the (012) face.

The crystal modeling program, WinXMorph, was used to build the crystal shape of the EDS crystal according to the indexed faces. To confirm the Miller index of the (012) crystal face obtained from calculation, the angle normal to this crystal face was obtained to be 56° using SHAPE (Figure 38).

Then using crystal drawing software a model of an EDS crystal with the indexed faces was created (Figure 39). These Miller indices provide the molecular presentation of EDS molecules at different crystalline faces.

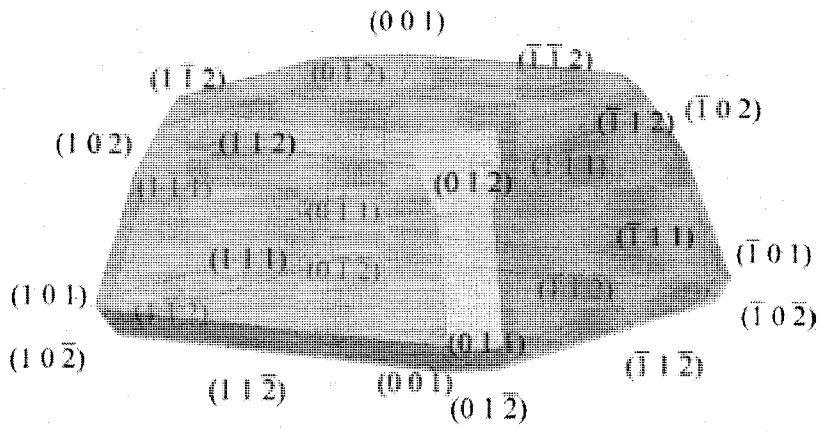

Figure 39. An indexed EDS crystal showing the major faces.

X-ray powder diffraction data was collected for EDS and the powder diffraction pattern obtained (Figure 40) was in agreement with the pattern calculated using the Mercury software (Table 6). Clearly, there are many smaller and/or hidden faces present in the EDS crystal.

This combined crystallographic information will be used to further study the process of directed chiral symmetry breaking of EDS at the molecular level.

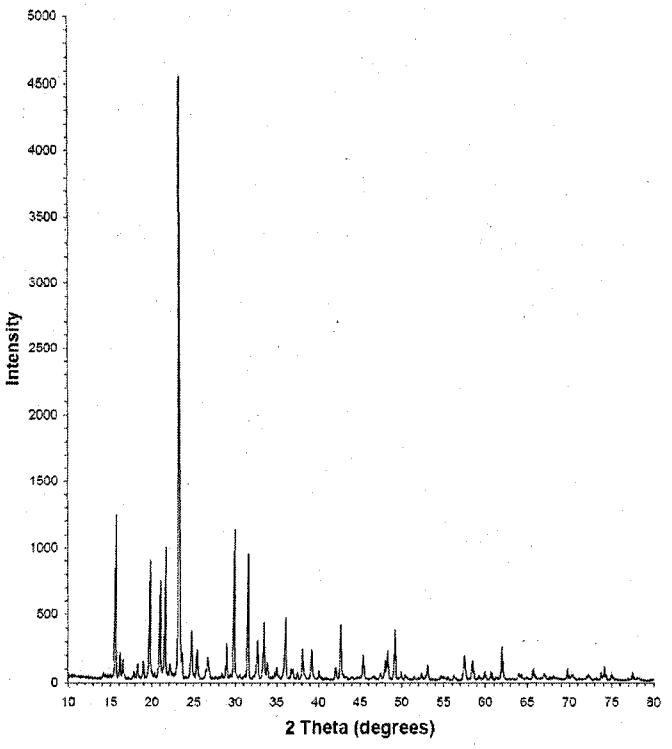

Figure 40. X-ray powder diffraction of EDS.

Table 6. X-ray data of EDS.

2θ exp (°)	hkl	I/Io	Δ2θ (°)*	2θ exp (°)	hkl	I/Io	Δ2θ (°)*
15.53	101	27.4	-0.03	49.03	312	8.5	0.01
18.01	102	1.3	0.03	49.81	225	1.8	-0.01
19.67	004	19.9	0.01	50.27	119	1.4	-0.01
20.89	110	16.5	-0.01	52.27	314	1.7	0.01
21.49	111	22.1	-0.01	52.99	218	2.8	0.01
23.15	112	100.0	0.05	54.59	3-15	1.3	-0.01
24.63	104	8.3	-0.03	54.99	209	1.2	-0.05
28.87	105	5.4	0.03	55.39	321	1.2	-0.01
29.77	200	24.4	0.01	56.13	322	1.3	-0.01
31.39	202	20.9	-0.01	57.33	3-16	4.5	-0.03
32.55	115	6.7	0.01	58.37	307	3.5	0.03
33.31	106	9.7	0.01	59.11	324	1.3	-0.03
33.75	2-11	3.3	0.01	59.83	228	1.9	0.03
34.87	212	2.3	0.01	60.55	3-17	1.8	0.01
35.93	204	9.9	0.01	61.83	400	5.8	0.03
36.59	116	2.2	-0.01	63.89	326	1.6	0.01
37.93	107	5.4	-0.05	64.17	411	1.3	0.01
39.05	205	5.0	0.03	65.57	404	2.2	0.03
39.91	008	2.0	-0.03	66.81	327	1.4	0.03
41.93	215	2.5	0.01	67.97	3-19	1.2	0.01
42.51	206	8.9	-0.01	69.63	4-15	2.3	0.03
45.25	216	4.5	-0.01	70.27	328	1.4	0.05
46.37	116	1.2	-0.03	72.07	4-23	1.5	-0.03
47.33	224	1.5	0.01	73.61	424	1.8	0.01
47.91	303	3.7	0.01	73.99	336	2.6	0.03
48.21	311	5.1	0.01	74.85	417	1.6	-0.01

* $\Delta 2\theta = 2\theta_{exp} - 2\theta_{calc}$

Chapter 4. Conclusions and future work

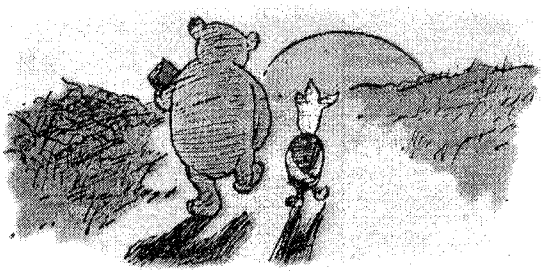

'Without Pooh,' said Rabbit solemnly as he sharpened his pencil, 'the adventure would be impossible.'

Winnie-the-Pooh

A.A. Milne

Our studies on the crystallization of ethylenediammonium sulfate demonstrated that: (*i*) complete asymmetric amplification of a 'racemic' mixture of an EDS sample can be achieved using an abrasion/grinding technique through an Ostwald ripening and recycling process and (*ii*) the direction of chiral symmetry breaking of EDS can be directed by the incorporation of chiral additives. Also, a model based on enantioselective adsorption was proposed to explain the directed chiral symmetry breaking process and the main crystalline faces of EDS crystals were indexed. This crystallographic information is crucial for future research on confirming the enantioselective adsorption of chiral amino acids on chiral EDS crystals using: (*i*) molecular modeling, (*ii*) surface etching, (*iii*) single molecular force spectroscopy and (*iv*) isothermal titration calorimetry.

Future research on confirming enantioselective adsorption on chiral EDS crystals will be conducted as follows:

(*i*) Molecular modeling will be performed on the (111) face in a water-mediated environment using the CHARMM software. The crystalline surface may be modeled as a flat surface or a surface containing steps or defects.

(*ii*) Surface etching on asymmetric EDS crystal faces with chiral amino acid solutions is expected to lead to the formation of asymmetric etch pits which would indicate enantioselective adsorption on particular crystal faces. Preliminary experiments carried out in our laboratory have shown that the angle of the etch pit axis of symmetry on the (111) face of a *d*-EDS crystal changes when etching with water, an L-amino acid solution or a D-amino acid solution. The more prominent angle demonstrates a stronger enantioselective adsorption of L-alanine on the (111) face of a *d*-EDS crystal compared to D-alanine on the same *d*-EDS crystal surface when viewed with the same orientated. This preliminary observation correlates with our result of directed symmetry breaking experiments and also our interpretation of data as shown in Figure 31. However, more experiments have to be performed to confirm the generality of this observation.

(*iii*) Single molecule force spectroscopy will be used to investigate the strength of binding of poly(amino acids) to various chiral crystalline surfaces of EDS. Poly(amino acids) will be covalently attached to an AFM tip and this modified tip will approach and retract from the chiral EDS crystal surfaces. A difference in plateau height in force extension curves for a poly(D-amino acid) interacting with a *dextrorotatory* EDS crystal surface compared to the profile for a poly(L-amino acid) on the same EDS crystal surface would provide a quantitative measure of enantioselective adsorption.

(*iv*) Isothermal titration calorimetry can be used to measure the enthalpy (ΔH) changes associated with enantioselective binding. This technique may provide valuable information on chiral amino acids adsorption on EDS crystal surfaces. A study of polymers binding to calcite crystals using this technique showed enantioselective adsorption effects during the titration measurements.[98] ITC experiments can be

performed by titrating chiral amino acid into a cell (working cell) containing powdered EDS crystals and the heat flow from this sample cell will be compared to a reference cell. In our case, the choice of solution medium is limited to any solvent system that will dissolve the desired amino acids but not the EDS crystallites. The resulting curve of heat per injected chiral amino acid (kJ mol^{-1}) versus the concentration of chiral amino acid (mM) may confirm the enantioselective adsorption of chiral amino acids on EDS crystals.

In this study, chiral amplification associated with the abrasion/grinding technique was used as a tool to investigate the enantioselective adsorption of amino acids to chiral crystals. If chiral selection is shown to occur on selective EDS surfaces then EDS crystals may have applications as a chiral platform for detecting extremely low enantiomeric excess in chiral molecules using the abrasion/grinding amplification technique. This, of course, would require starting with a truely racemic mixture of EDS.

Finally, it is believed that the work presented in this thesis provides an important contribution towards a better understanding of homochirogenesis. By using the abrasion/grinding chiral amplification technique, our results suggest an enantioselective adsorption mechanism of chiral biologically relevant molecules at chiral EDS crystalline surfaces. The fact that EDS is itself an achiral molecule in solution makes our findings more intriguing with regards to the origins of homochirality.

References

[1] L. E. Orgel, *Trends Biochem. Sci.* **1998**, *23*, 491-495.

[2] N. Lahav, *Biogenesis: Theories of Life's Origin*, Oxford University Press, Inc., New York, **1999**.

[3] R. M. Hazen, in *Genesis: The Scientific Quest for Life's Origin*, Joseph Henry Press, Washington, DC, **2005**, pp. 205-214.

[4] R. M. Hazen, in *Genesis: The Scientific Quest for Life's Origin*, Joseph Henry Press, Washington, DC, **2005**, pp. 215-219.

[5] G. H. Wagnière, *On Chirality and the Universal Asymmetry: Reflections on Image and Mirror Image*, WILEY-VCH, Zürich, Switzerland, **2007**.

[6] T. D. Lee, C. N. Yang, *Phys. Rev.* **1956**, *104*, 254-258.

[7] C. S. Wu, E. Ambler, R. W. Hayward, D. D. Hoppes, R. P. Hudson, *Phys. Rev.* **1957**, *105*, 1413-1415.

[8] J. R. P. Angel, R. Illing, *Nature* **1972**, *238*, 389-390.

[9] R. D. Wolstencroft, in *The Search for Extraterrestrial Life: Recent Developments* (Ed.: M. D. Papagiannis), D. Reidel Publishing Company, Boston, **1985**, pp. 171-175.

[10] J. R. Cronin, S. Pizzarello, D. P. Cruikshank, in *Meteorites and the Early Solar System* University of Arizona Press, Tucson, **1988**, pp. 819-857.

[11] Y. Wolman, W. J. Haverland, S. L. Miller, *Proc. Natl. Acad. Sci.* **1972**, *69*, 809-811.

[12] W. A. Bonner, P. R. Kavasmaneck, F. S. Martin, J. J. Flores, *Origins of Life* **1975**, *6*, 367-376.

[13] R. M. Hazen, T. R. Filley, G. A. Goodfriend, *Proc. Natl. Acad. Sci.* **2001**, *98*, 5487-5490.

[14] A. M. Cody, R. D. Cody, *J. Cryst. Growth* **1991**, *113*, 508-519.

[15] R. M. Hazen, *Elements* **2005**, *1*, 135-137.

[16] E. L. Eliel, S. H. Wilen, M. P. Doyle, *Basic Organic Stereochemistry*, John Wiley & Sons, Inc., New York, **2001**.

[17] R. S. Cahn, C. Ingold, V. Prelog, *Angew. Chem., Int. Ed. Engl.* **1966**, *5*, 385-415.

[18] E. Fischer, O. Piloty, *Ber. Chem. Ges.* **1891**, *24*, 521.

[19] T. M. Lowry, *Optical Rotatory Power*, Dove Publications, New York, **1964**.

[20] L. Pasteur, in *Leçons de Chimie Professées en 1860; Société Chimique de Paris: Paris 1861, Vol. 14*, William F. Clay, Edinburgh, **1897**, pp. 7-46.

[21] D. G. Morris, *Basic Concepts in Chemistry*, Wiley-Interscience: Royal Society of Chemistry, New York, **2002**.

[22] C. Hammond, *The Basic of Crystallography and Diffraction*, Second ed., Oxford University Press, New York, **2001**.

[23] F. C. Phillips, *An Introduction to Crystallography*, 3rd ed., Longmans, London, **1963**.

[24] D. E. Sands, *Introduction to Crystallography*, W. A. Benjamin, Inc., New York, **1969**.

[25] I. Sunagawa, *Crystals: Growth, Morphology and Perfection*, Cambridge University Press, New York, **2005**.

[26] L. Addadi, Z. Berkovitch-Yellin, I. Weissbuch, J. v. Mil, L. J. W. Shimon, M. Lahav, L. Leiserowitz, *Angew. Chem. Int. Ed. Engl.* **1985**, *24*, 466-485.
[27] W. Kaminsky, E. Haussuhl, L. D. Bastin, J. Anand Subramony, B. Kahr, *J. Cryst. Growth* **2002**, *234*, 523-528.
[28] A. Mauri, M. Moret, *J. Cryst. Growth* **2000**, *208*, 599-614.
[29] C. A. Orme, A. Noy, A. Wierzbicki, M. T. McBride, M. Grantham, H. H. Teng, P. M. Dove, J. J. DeYoreo, *Nature* **2001**, *411*, 775-779.
[30] J. Applequist, *Am. Sci.* **1987**, *75*, 59-68.
[31] J. D. Dana, E. S. Dana, *The System of Mineralogy*, 7th ed., John Wiley and Sons, Inc., New York, **1962**.
[32] O. B. Ramsay, in *Nobel Prize Topics in Chemistry: Stereochemistry* (Ed.: J. W. van Spronsen), Heyden, London, **1981**, p. 256.
[33] G. B. Kauffman, R. D. Myers, *J. Chem. Educ.* **1975**, *52*, 777-781.
[34] M. Avalos, R. Babiano, P. Cintas, J. L. Jimenez, J. C. Palacios, *Tetrahedron: Asymmetry* **2004**, *15*, 3171-3175.
[35] D. K. Kondepudi, K. Asakura, *Acc. Chem. Res.* **2001**, *34*, 946-954.
[36] S. C. Abrahams, J. L. Bernstein, *Acta Crystallogr., Sect. B: Struct. Crystallogr. Cryst. Chem.* **1977**, *B33*, 3601-3604.
[37] J. Szurgot, M. Szurgot, *Cryst. Res. Technol.* **1995**, *30*, 71-79.
[38] J. Jacques, A. Collet, S. H. Wilen, *Enantiomers, Racemates, and Resolutions*, John Wiley & Sons, New York, **1981**.
[39] F. S. Kipping, W. J. Pope, *J. Chem. Soc., Trans.* **1898**, *73*, 606.
[40] D. K. Kondepudi, R. J. Kaufman, N. Singh, *Science* **1990**, *250*, 975-977.
[41] D. K. Kondepudi, K. L. Bullock, J. A. Digits, J. K. Hall, J. M. Miller, *J. Am. Chem. Soc.* **1993**, *115*, 10211-10216.
[42] J. H. E. Cartwright, J. M. Garcia-Ruiz, O. Piro, C. I. Sainz-Diaz, I. Tuval, *Phys. Rev. Lett.* **2004**, *93*, 035502/035501-035502/035504.
[43] C. I. Sainz-Diaz, A. P. Martin-Islan, J. H. E. Cartwright, *J. Phys. Chem. B* **2005**, *109*, 18758-18764.
[44] R. E. Pincock, R. R. Perkins, A. S. Ma, K. R. Wilson, *Science* **1971**, *174*, 1018-1020.
[45] D. K. Kondepudi, J. Laudadio, K. Asakura, *J. Am. Chem. Soc.* **1999**, *121*, 1448-1451.
[46] C. Viedma, *Phys. Rev. Lett.* **2005**, *94*, 065504/065501-065504/065504.
[47] C. Viedma, *Los Alamos National Laboratory, Preprint Archive, Condensed Matter* **2005**, 1-5, arXiv:cond-mat/0507347.
[48] Y. Song, W. Chen, X. Chen, *Cryst. Growth Des.* **2008**, *8*, 1448-1450.
[49] J. H. E. Cartwright, O. Piro, I. Tuval, *Phys. Rev. Lett.* **2007**, *98*, 165501/165501-165501/165504.
[50] C. Viedma, *Total chiral symmetry breaking by bifurcation from racemic systems: when "left" and "right" cannot coexist.* http://arxiv.org/ftp/cond-mat/papers/0407/0407479.pdf
[51] C. Viedma, *Cryst. Growth Des.* **2007**, *7*, 553-556.
[52] T. Niedermaier, W. Schlenk, Jr., *Chem. Ber.* **1972**, *105*, 3470-3478.
[53] O. Vogl, M. Qin, J. Bartus, G. D. Jaycox, *Monatsh. Chem.* **1995**, *126*, 67-73.

[54] S. J. George, Z. Tomovic, M. M. J. Smulders, T. F. A. de Greef, P. E. L. G. Leclere, E. W. Meijer, A. P. H. J. Schenning, *Angew. Chem., Int. Ed.* **2007**, *46*, 8206-8211.
[55] E. Kolomiets, V. Berl, J.-M. Lehn, *Chem. Eur. J.* **2007**, *13*, 5466-5479.
[56] M. Szurgot, *Cryst. Res. Technol.* **1995**, *30*, 621-628.
[57] R. M. Hazen, in *Progress in Biological Chirality* (Ed.: G. P. C. Z. L. Caglioti), Oxford: Elsevier, **2004**, pp. 137-151.
[58] R. M. Hazen, *Am. Mineral.* **2006**, *91*, 1715-1729.
[59] P. F. Hoffman, *The Geology of North America; An Overview, Vol. A*, The Geological Society of America, Inc., Boulder, **1986**.
[60] R. M. Hazen, D. S. Sholl, *Nat. Mater.* **2003**, *2*, 367-374.
[61] L. Addadi, Z. Berkovitch-Yellin, N. Domb, E. Gati, M. Lahav, L. Leiserowitz, *Nature* **1982**, *296*, 21-26.
[62] B. Kahr, J. K. Chow, M. L. Peterson, *J. Chem. Educ.* **1994**, *71*, 584-586.
[63] B. Kahr, L. Vasquez, *Cryst. Eng. Comm.* **2002**, *4*, 514-516.
[64] B. Kahr, R. W. Gurney, *Chem. Rev.* **2001**, *101*, 893-951.
[65] S. A. de Vries, P. Goedtkindt, S. L. Bennett, W. J. Huisman, M. J. Zwanenburg, D. M. Smilgies, J. J. De Yoreo, W. J. P. van Enckevort, P. Bennema, E. Vlieg, *Phys. Rev. Lett.* **1998**, *80*, 2229-2232.
[66] W. M. Vetter, H. Totsuka, M. Dudley, B. Kahr, *J. Cryst. Growth* **2002**, *241*, 498-506.
[67] L. D. Bastin, B. Kahr, *Tetrahedron* **2000**, *56*, 6633-6643.
[68] I. Ojima, *Catalytic asymmetric synthesis*, 2nd ed., John Wiley & Sons, Inc., New York, **2000**.
[69] M. Sakamoto, S. Kobaru, T. Mino, T. Fujita, *Chem. Commun.* **2004**, 1002-1003.
[70] K. Soai, T. Shibata, H. Morioka, K. Choji, *Nature* **1995**, *378*, 767-768.
[71] J. J. Flores, W. A. Bonner, G. A. Massey, *J. Am. Chem. Soc.* **1977**, *99*, 3622-3625.
[72] T. Shibata, J. Yamamoto, N. Matsumoto, S. Yonekubo, S. Osanai, K. Soai, *J. Am. Chem. Soc.* **1998**, *120*, 12157-12158.
[73] K. Soai, S. Osanai, K. Kadowaki, S. Yonekubo, T. Shibata, I. Sato, *J. Am. Chem. Soc.* **1999**, *121*, 11235-11236.
[74] I. Sato, K. Kadowaki, K. Soai, *Angew. Chem., Int. Ed.* **2000**, *39*, 1510-1512.
[75] I. Sato, K. Kadowaki, Y. Ohgo, K. Soai, *J. Mol. Catal. A: Chem.* **2004**, *216*, 209-214.
[76] T. Kawasaki, M. Sato, S. Ishiguro, T. Saito, Y. Morishita, I. Sato, H. Nishino, Y. Inoue, K. Soai, *J. Am. Chem. Soc.* **2005**, *127*, 3274-3275.
[77] D. G. Blackmond, *Chem. Eur. J.* **2007**, *13*, 3290-3295.
[78] W. Meyerhoffer, *Ber. Dtsch. Chem. Ges.* **1904**, *37*, 2604-2610.
[79] W. L. Noorduin, T. Izumi, A. Millemaggi, M. Leeman, H. Meekes, W. J. P. Van Enckevort, R. M. Kellogg, B. Kaptein, E. Vlieg, D. G. Blackmond, *J. Am. Chem. Soc.* **2008**, *130*, 1158-1159.
[80] M. Klussmann, H. Iwamura, P. Mathew Suju, H. Wells David, Jr., U. Pandya, A. Armstrong, G. Blackmond Donna, *Nature* **2006**, *441*, 621-623.
[81] D. G. Blackmond, M. Klussmann, *Chem. Commun.* **2007**, 3990-3996.

[82] M. Klussmann, J. P. White Andrew, A. Armstrong, G. Blackmond Donna, *Angew. Chem., Int. Ed. Engl.* **2006**, *45*, 7985-7989.
[83] R. H. Perry, C. Wu, M. Nefliu, R. G. Cooks, *Chem. Commun.* **2007**, 1071-1073.
[84] S. P. Fletcher, R. B. C. Jagt, B. L. Feringa, *Chem. Commun.* **2007**, 2578-2580.
[85] K. Jayaraman, A. Choudhury, C. N. R. Rao, *Solid State Sci.* **2002**, *4*, 413-422.
[86] P. Groth, *Chemische Kristallographie, Vol. 3*, Leipzig, Engelmann, **1910**.
[87] A. Holden, P. Singer, *Crystals and Crystal Growing*, Anchor Books, Garden City, N.Y., **1960**.
[88] B. R. Brooks, R. E. Bruccoleri, B. D. Olafson, D. J. States, S. Swaminathan, M. Karplus, *J. Comput. Chem.* **1983**, *4*, 187-217.
[89] W. R. Cannon, B. M. Pettitt, J. A. McCammon, *J. Phys. Chem.* **1994**, *98*, 6225-6230.
[90] R. E. Bruccoleri, M. Karplus, *J. Comput. Chem.* **1986**, *7*, 165-175.
[91] L. Koby, J. B. Ningappa, M. Dakessian, L. A. Cuccia, *J. Chem. Educ.* **2005**, *82*, 1043-1045.
[92] C. Viedma, *Astrobiol.* **2007**, *7*, 312-319.
[93] P. S. M. Cheung, J. Gagnon, J. Surprenant, Y. Tao, H. Xu, L. A. Cuccia, *Chem. Commun.* **2008**, 987-989.
[94] C. Viedma, *Los Alamos National Laboratory, Preprint Archive, Condensed Matter* **2004**, 1-8, arXiv:cond-mat/0407479.
[95] V. A. Davankov, *Chirality* **1997**, *9*, 99-102.
[96] V. Prelog, *Science* **1976**, *193*, 17-24.
[97] A. Kuhnle, R. Linderoth Trolle, B. Hammer, F. Besenbacher, *Nature* **2002**, *415*, 891-893.
[98] R. Dimova, R. Lipowsky, Y. Mastai, M. Antonietti, *Langmuir* **2003**, *19*, 6097-6103.

The End